CHALMERS
UNIVERSITY OF TECHNOLOGY

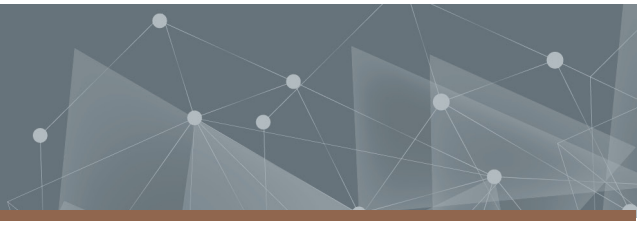

Towards In-Line Detection of Milk Spoilage Using Nuclear Magnetic Resonance

Master's Thesis in Material's Chemistry

Olle Hildebrand

DEPARTMENT OF, CHEMISTRY AND CHEMICAL ENGINEERING

CHALMERS UNIVERSITY OF TECHNOLOGY
Gothenburg, Sweden 2026
www.chalmers.se

Master's thesis 2026

Towards In-Line Detection of Milk Spoilage Using Nuclear Magnetic Resonance

Olle Hildebrand

CHALMERS
UNIVERSITY OF TECHNOLOGY

Department of Chemistry and Chemical Engineering
Division of Applied Chemistry
Chalmers University of Technology
Gothenburg, Sweden 2026

Towards In-Line Detection of Milk Spoilage Using Nuclear Magnetic Resonance
Olle Hildebrand

Supervisor: Diana Bernin, Chemistry and Chemical Engineering
Examiner: Diana Bernin, Chemistry and Chemical Engineering

Master's Thesis 2026
Department of Chemistry and Chemical Engineering
Division of Applied Chemistry
Chalmers University of Technology
SE-412 96 Gothenburg
Telephone +46 31 772 1000

Typeset in LaTeX
Printed by Chalmers Digital Printing
Gothenburg, Sweden 2026

Towards In-Line Detection of Milk Spoilage Using Nuclear Magnetic Resonance
OLLE HILDEBRAND
Department of Chemistry and Chemical Engineering
Chalmers University of Technology

Abstract

Milk is one of the most important foods in the world, consumed by over 6 billion people annually. Its nutrient rich content makes it a complete food source, however this also leads to that microorganisms can thrive inside the milk. This causes spoilage and the milk can no longer be sold to the consumers. This thesis investigates a new method to detect milk spoilage using NMR. The method would be able to be used as an in-line process and would increase the amount of tested products.

Three different microorganisms were studied, *Leuconostoc mesenteroides, Exiguobacterium undae*, and *Pseudomonas chlororaphis*. For each microorganism NMR spectroscopy, relaxation times and diffusion were measured by three different instruments and magnetic field strengths, 300 MHz MRI, 60 MHz NMR and 20 MHz TD-NMR. The values were extracted by fitting signal models and the overall trends were observed. Packaging materials effects on the signal-to-noise ratio of the NMR signal and on the relaxation times were also studied at 20 MHz to understand the potential of using low-field NMR in industry.

Diffusion experiments showed low potential for industry use due to lacking significant differences for treated and non-treated samples. For T_2 clear overall trends could not be observed and microorganisms dependent trends were more clear. T_2 showed significantly lower standard deviation than T_1 making it interesting for future research. On the other hand, T_1 showed the most overall clear trends with an increase over time indicating that the chemical environment is changing due to contamination. The complexity of milk spoilage made it difficult to determine which relaxation time was best indicator for spoilage, but it demonstrated how NMR signals are affected by milk spoilage.

More research needs to be done to build on the findings of this thesis, specifically with more replicates and focusing on a specific instrument. Results from packaging material experiments demonstrated how it would not be the hindering factor for an in-line process, it showed that low-field NMR signals could be detectable through materials, even with an aluminium layer.

The thesis provided a broader understanding of milk spoilage, its causes and how it affects relaxation times and spectra. All three microorganisms showed similar trends for all instruments suggesting that general spoilage mechanisms can be detected even if the underlying microorganisms differ. The results suggest that low-field NMR could be a viable method for milk spoilage detection.

Keywords: NMR, Milk Spoilage, Food Safety, In-Line Detection, Microorganisms.

Acknowledgments

I would like to express my sincere gratitude to my supervisor, Diana Bernin, for her guidance and support throughout this thesis. I would also like to thank Tetra Pak for their collaboration. In particular, I am grateful to Nikoleta Zeaki, Martin Lappann, and João Pedro De Almeida Martins for their assistance, insightful discussions, and support during the project. Finally, I would like to thank my family and friends for their support and encouragement throughout this project.

Olle Hildebrand, Gothenburg, May 2026

List of Acronyms

Below is the list of acronyms that have been used throughout this thesis listed in alphabetical order:

ADC	Apparent Diffusion Coefficient
AIC	Akaike Information Criterion
ATP	Adenosine Triphosphate
BIC	Bayesian Information Criterion
CFU	Colony Forming Units
CPMG	Carr-Purcell-Meiboom-Gill
IR	Inversion Recovery
MRI	Magnetic Resonance Imaging
MSME	Multi-Slice Multi-Echo
NMR	Nuclear Magnetic Resonance
ppm	parts per million
PRESS	Point RESolved Spectroscopy
RARE VTR	Rapid Acquisition with Relaxation Enhancement at Variable TR
RF	Radio Frequency
RLU	Relative Light Unit
RMSE	Root Mean Square Error
SD	Standard Deviation
SE	Spin Echo
SNR	Signal to Noise Ratio
TD-NMR	Time Dependent Nuclear Magnetic Resonance
TE	Echo Time
TR	Repetition Time
UHT	Ultra High Temperature
WET	Water Suppression Enhanced

Nomenclature

Below is the nomenclature of parameters and variables that have been used throughout this thesis.

Parameters

β	Stretching component
γ	Gyromagnetic ratio
$\Gamma(k)$	Gamma function
$\hbar$	Reduced Planck's constant
μ	Magnetic moment

Variables

A	Amplitude
B_0	External magnetic field
C	Constant offset for background noise
ΔE	Energy difference between two energy states
I	Quantum number
k	Shape parameter
S	Nuclear spin
S_∞	Estimated equilibrium signal
T_1	Longitudinal relaxation time
T_2	Transverse relaxation time
τ	Characteristic relaxation time
θ	Scaling parameter

Contents

List of Figures

List of Tables

1
Introduction

Milk is one of the most consumed food products around the world with over 6 billion people consuming it every year [1]. Milk is often considered as one of the most complete foods found in nature [2] but it is also very vulnerable to contamination and spoilage due to its nutrient-rich environment where microorganism and bacteria can thrive [3]. Ultra High Temperature (UHT) milk is an alternative to the milk products often found in Swedish supermarkets which is heated up to 135°C to sterilize and kill the bacteria in the milk [4]. This type of milk product has a large part of the global sector due to its shelf stable properties. UHT milk is often found in countries with warmer climates where refrigerated storage is limited or more expensive. This is because it delivers a cost effective and safe way to distribute milk over different countries and climates.

However, because it is a shelf stable product one of the largest problems it faces is contaminations during the production process. After the treatment to become UHT milk it is packaged in aseptic packaging to minimize contaminants in the milk [4]. Contaminants are still sometimes prevalent in the finished packages [3] on its way to the consumers that will only be visible after several days or longer of incubation in the packages. Today only a small amount of the packages are able to be tested to prevent contaminates as the package needs to be opened to conduct a test on the milk.

The largest producer of these products is Tetra Pak, and together with them this thesis will investigate if there is a better way to test for contaminants in milk. A non-destructive test method that could be implemented into an in-line would be the best option.

The aseptic testing methods currently in use are destructive in nature, meaning that the milk that is tested cannot be sold anymore. A potential non-destructive alternative is the use of Nuclear Magnetic Resonance (NMR), which will be investigated in this thesis. NMR is already of use in other areas of food science [5] but to be able to use it in a milk production process is a new area which could change how we look for contaminants in milk production. When milk is contaminated microorganism will thrive in the milks environment due to the high levels of organics [3]. The fat, proteins and lactose of milk can in some cases be broken down to new products which will reflect in the NMR signals.

By using the NMR data from a reference sample without contaminants, together with a contaminated milk sample it could be able to detect for contaminants. The strength of NMR would also make it possible to only focus on relaxation times to detect the contaminants. Using relaxation times will also open up the possibility of using low-field NMR which is both cheaper and easier to use in industry.

Milk is one of the most wasted foods in the world with 7-15 % of milk for consumption wasted each year in the western world [6]. The high amount of waste can be directly linked to the shelf life of milk according to a study in the UK [7]. By introducing the possibility to widen the reach of shelf stable milk will reduce the overall waste. A contaminate free milk with a simplified analysing system is the most important step towards this and could change the way milk is processed. Using a non-destructive test method in an in-line process would enable testing of all products before going out to consumers. This would increase the efficiency of the process and minimize the waste created by testing products to nearly zero.

1.1 Aim

The overall aim of the thesis is to evaluate the potential of using NMR techniques to detect milk spoilage. Preliminary MRI results showed that nuclear magnetic resonance methodology is a promising tool to detect milk spoilage, which is the basis for this thesis. The focus of this thesis is to gain fundamental knowledge using different NMR techniques to identify what changes are happening during spoilage and how they are impacting the NMR signal. It aims to test samples of UHT milk which have been exposed to three microorganisms, *Leuconostoc mesenteroides, Exiguobacterium undae* and *Pseudomonas chlororaphis*. These microorganisms were chosen and provided by Tetra Pak. Three different instruments with three field strengths will be compared, 300 MHz MRI, 60 MHz NMR and a 20 MHz TD-NMR. From this testing it will be possible to understand how spoilage in dairy products can be detected. But also what happens in the product when contaminants or microorganisms are introduced. The results from those tests gives insight into the feasibility to devise a future in-line procedure for detecting milk spoilage within Tetra Pak's industrial processes.

2
Theory

This chapter covers the theoretical background relevant for the thesis. Firstly it explains the analysis methods in use today, further it discusses the different milk spillages that can occur. The three microorganisms and their respective microbial mechanisms and how they could affect the chemical structure and measured signals from milk is demonstrated. It also covers the theoretical background for MRI, NMR and the mathematical models used for fitting the data obtained from measurements.

2.1 Milk

Milk is mainly composed of water with a total of 85-90 %, the remaining 10% consists of carbohydrates (Lactose), fats and proteins. It is also an important source of nutrients such as magnesium, calcium and other nutrients that are of important for the human body to function at a good level. Cow milk normally has a distribution of 3-4% of fat, 3.5% of proteins and a lactose concentration of 5% [8].

The fat content of milk can vary between different animals and breeds of cows, however in the production of milk the fat percentage is altered to fit the consumers preference. Whole milk remains at the standard level of cow milk fats at 3-4% while skimmed and semi-skimmed has the fat removed to reach a level of 2% and nearly 0%. In raw milk the fats are dispersed in the water as an emulsion, and the fat and water would therefore eventually separate if left alone. To prevent this milk homogenization is used to create a stable emulsion [9] to improve the drinking experience of the milk but it also improves the overall flavour and colour of the milk. To homogenize the milk, it is put through a small gap between two steel plates which breaks down the larger fat globule to create a more stable emulsion with smaller fat globules dispersed in the water [9].

Milk proteins are divided into two different protein fractions: casein and whey. Casein is a slow digesting protein which accounts for 80% while whey is a faster digesting protein which accounts for 20% of all proteins [10]. Together they provide all nine essential amino acids and therefore milk is a high quality source of protein.

Lactose is a type of milk sugar and is the most prevalent carbohydrate found in milk. Lactose is a disaccharide composed of glucose and galactose. The market for lactose free products is growing fast as the health awareness around the world is increasing [11]. Over 70% of the world experiences lactose malabsorption which is a deficiency of the enzyme lactase which breaks down the milk sugar. However, lactose plays an important role in specifically infants' diet where it is beneficial for their development [12].

The nutrition rich composition of milk provides a great environment for microbes that can lead to spoilage of the product. Therefore, microbes need to be eliminated from the product and prevented from re-entering the product. Alternatively, the product must be chilled to keep microbes from growing in the product [13] [3]. Microbial activity can lead to milk spoilage through three mechanisms: physical, chemical or microbial spoilage [14].

The microorganisms can create enzymes that break down the proteins, lactose and fats and alter the pH of the milk leading to chemical spoilage. Physical spoilage is caused by microbial growth which changes the appearance and texture of the milk, such as gas formation and curdling [3]. Microbial spoilage is due to the microorganism which causes safety and health concerns by promoting growth of bacteria.

2.2 Ultra High Temperature (UHT) Milk

UHT milk is an alternative to standard milk which has several different benefits compared to the milk often seen in Sweden. The purpose of UHT treatment is to completely eliminate any microorganism who would be able to grow in the product under normal storage and distribution conditions. Therefore it does not need to be refrigerated to control microbes, and is shelf stable for longer. These properties have made the UHT milk a common choice for commercial kitchens and other countries around the world. To obtain these desired properties the milk is sterilized at a minimum of 135°C for a few seconds which results in a commercially sterile product which is free of all microorganisms [4]. The milk is thereafter packaged in aseptic packaging to keep the product commercially sterile and hinder any microorganism from re-entering the product.

The demand for UHT milks has increased significantly in the last 20 years and is expected to keep growing at 5 % per year over the next 10 years [15]. The UHT milk products market accounts for a significant segment of the diary market and accounts for approximately 18-20% of the overall market. The heat treatment used for UHT milk could reduce the amount of heat sensitive nutrients. The longer storage time possible with this type of milk might also degrade some of the nutrients over long time periods [4]. However, the main components and overall nutritional value of the two different types of milk remain the same.

2.3 Analysis Method in Use

During the process of milk collection, processing, packaging and distribution, microbes can make their way into the finished product and cause spoilage. The microbes can originate from the raw milk and survive during the processing, or they can be introduced into the product after processing during the packaging or distribution of the product [3]. Commercial release of UHT milk requires documented process control and microbiological analysis of a fraction of the produced packages to verify that widespread microbiological contamination has not occurred and that the product is safe for consumers. Current microbiological end-product evaluation methods are destructive: packages must be opened, emptied, and sampled to determine whether they are contaminated or commercially sterile. Because tested packages must be discarded, destructive sterility testing creates both cost and waste. As a result, only a small fraction of the total production can be tested. This chapter covers the most frequently used destructive commercial sterility methods.

2.3.1 Traditional Methods

Traditional methods used for milk analysis are often seen as slow but reliable. During contamination of UHT milk and connected milk spoilage organic acids are formed from the bacterial growth of bacteria which can lower the pH of the product [3]. The pH decrease associated with microbial contamination is used as a means of distinguishing between commercially sterile products and microbiologically contaminated products using pH measurements. UHT milk has an industry standard pH value of 6.6 [3][14]. Since there are no physical or chemical processes occurring in milk after filling that could significantly lower the pH, a lowering of the product's pH after pre-incubation indicates that the UHT milk is microbiologically contaminated. For reliable pH drop, contaminants need to grow to high cell densities which requires long pre-incubation time.

Streak plating is another frequently used commercial sterility test method which also allows identifying the species of contaminants. This is beneficial for the root cause finding of the contamination and for judging potential hazards to the health of consumers. In comparison to pH testing, streak plating also relies on sufficiently long pre-incubation time to ensure fully grown microbial streaks but this method requires lower cell densities than pH measurement requires. A small product sample is streaked on an Agar plate and is then left to incubate for growth. During this time each microorganism grows into one colony forming unit (CFU) and produces an isolated colony. [16]. These CFUs can be observed and counted to identify the bacteria and its concentration.

2.3.2 Rapid Test Methods

Other methods have been invented to decrease the time needed for detection. These methods are also used in industries and as a compliment to the traditional methods. ATP bioluminescence uses the ATP naturally found in organisms for energy storage to be able to detect contaminants [17]. ATP is present in all living cells and by adding the enzyme luciferase, a catalytic reaction occurs releasing light. This light can be captured and quantified as relative light units (RLU) which can be directly correlated with the amount of metabolically active microorganisms. For the method to be effective non-microbial ATP needs to be removed from the product samples while preserving the microbial ATP. The technique offers high sensitivity and speed combined with the ability to detect microorganisms at lower concentrations [17]. These properties make ATP bioluminescence a very useful technique in commercial sterility testing.

Colorimetric growth detection is another commercial sterility test method that relies on colour changes induced by pH change or carbon dioxide release upon microbial contamination on a colour indicator added to the product [17]. Microbial growth changes will result in a colour change which can be visually observed or continuously monitored by an instrument. Another method to determine commercial product sterility is flow cytometry. Here, a substrate is added to a product sample and is taken up and converted by microbes into a fluorochrome which turns respective microbes fluorescent upon proper excitation by a laser. The fluorescent microbes in a product sample can be detected and counted [18].

2.4 Microorganisms

The composition of milk with fats, proteins, carbohydrates and a wide array of nutrients enables bacterial growth [13]. The microbes can originate from different parts of the process, for instance, some microbes are coming from the cow's mammary glands [19]. There is not only microbes coming from the cow itself there is also microbes introduced to the milk through handling and equipment used for the processing further on after extracting the milk from the cows [3] [19]. Understanding where these microbes come from and how they could spoil the milk is of importance to identify the most likely point of entry of microorganisms into the UHT milk production process.

These microorganisms are often not inherently dangerous to people with healthy immune systems, but can lead to rare infections upon consumption of microbiologically contaminated products. [20]. During this project three prevalent microbial contaminants leading to spoilage of milk were studied.

2.4.1 Leuconostoc Mesenteroides

Leuconostoc mesenteroides is a Gram-positive bacterium, a part of the lactic acid bacteria and is often used in fermentation. Its primary effect on milk is through carbohydrate metabolization of lactose or other carbohydrates present. The lactose is converted through fermentation to organic acids, lactic acid and acetate [19], which results in a large drop in pH from industry standard 6.6 to down to 4.5 [3]. Due to the drop in pH the casein micelles can start to destabilize and aggregate due to it reaching the iso electric point of casein, resulting in strong milk coagulation [19].

The bacterium does not release proteases and does not show proteolytic activity to degrade casein. It also does not show any esterase or lipase activity and therefore cannot break down milk fats. The carbohydrate metabolisms connected to acid release can be beneficial in controlled dairy fermentation [19]. However, it is also associated with milk spoilage when unintentionally introduced into commercially sterile UHT milk during re-contamination.

2.4.2 *Exiguobacterium Undae*

Exiguobacterium undae is a Gram-positive bacterium that is found in different environments such as water and soil. *E. undae* exhibits proteolytic activity through its production of protease [21], and breaking down casein into peptides [3]. The protein degradation that occurs is generally less pronounced in visible structural changes in the milk. Similar to *L. mesenteroides* it does not exhibit any lipase activity and has therefore no effect on the fats or rancid flavour often connected to lipolytic spoilage.

E. undae produces organic acids from carbohydrates, but it does not utilize lactose for this purpose. Lactose being the main carbohydrate in milk the acid production for *E. undae* will only show a moderate pH drop. Coagulation of the milk is often not seen as the pH does not drop enough to destabilize the casein micelles. The impact of *E. undae* is characterized by low acidification and low proteolytic activity without any major structural changes.

2.4.3 *Pseudomonas Chlororaphis*

Pseudomonas chlororaphis is a Gram-negative bacterium connected with soil and water contamination [3] and spoilage of refrigerated milk. Milk spoilage upon microbial contamination is primarily linked to enzymatic breakdown in milk products rather than fermentation. Proteolytic activity is exhibited through production of protease similar to *E. undae* and breaks down casein to smaller peptides. Protease can affect the texture of the milk [3] but is often not able to be observed visually and usually there is no coagulation present in the milk.

P. chlororaphis does primarily show esterase activity and might also show lipase activity from lipolysis. This results in rancidity in the milk due to the release of volatile fatty acids [3]. This bacterium does not utilize lactose for carbohydrate metabolism and no formation of organic acids or pH drop should be expected. *P. chlororaphis* contributes mainly to the spoilage of milk through enzymatic degradation. Some members of the genus *Pseudomonas* have the ability to grow at low temperatures and some enzymes can remain active in the product even after pasteurization or UHT treatment despite the killing of the Pseudomonas bacteria itself [19].

2.5 Nuclear Magnetic Resonance (NMR)

NMR is one of the most used and powerful spectroscopy techniques used to determine physical, chemical and biological properties and structure of molecules. NMR is a non-destructive reproducible technique that is able to detect multiple compounds in a single measurement of a sample [22].

NMR signal is given from nuclei absorbing specific radio frequencies exciting the nuclear spin. Magnetic resonance explains how atomic nuclei emit electronic radiation when placed in an external magnetic field. Nuclei with spin aligns with or against the magnetic field creating different energy levels [23]. The nuclei absorb energy to transition between the different spin states. After excitation they return to equilibrium where a detectable signal is measured, which is used to obtain information about the structure of the molecules.

The nuclei must have a non-zero spin quantum number $I \neq 0$ to be observed, nuclei with I=0 do not have any magnetic moment and are therefore invisible in the NMR spectrum [23]. The magnetic moment (μ) is proportional to the nuclear spin (S), as given by the Equation 2.1, where γ is the gyromagnetic ratio which represents how strong a specific nucleus interacts with an external field.

$$\mu = \gamma \cdot S \tag{2.1}$$

When an external field (B_0) is applied to a nucleus with spin I=1/2 split into the two energy states $\pm\frac{1}{2}$. The energy difference between the two energy states allows the nuclei to absorb electromagnetic radiation at a specific frequency. The energy difference is proportional to the magnetic field by Equation 2.2, where $\hbar = \frac{h}{2\pi}$ (reduced Planck constant).

$$\Delta E = \gamma \hbar B_0 \tag{2.2}$$

The abundance of water molecules in milk causes problems in analysing the results as the peaks that are of interest become minuscule and the accuracy of the measurements is decreased [24]. To combat this problem water suppression can be used in the instrument to be able to analyse the peaks that are of interest.

Shimming
The applied magnetic field needs to be calibrated before usage to be homogeneous [25]. This enhances the water suppression which is of high importance when looking at samples with a large water component. Implementing shimming narrows the peaks width and enhances the signal to noise ratio (SNR) which improves the sensitivity and resolution [25]. Shimming is done by adjusting the current in the coils to cancel out the fields inhomogeneities.

Chemical shift
The chemical shift in NMR describes how different chemical environment varies the resonance frequency of a nucleus. It's expressed in ppm and is the relative difference in resonance frequency between nuclei in different chemical environments [23]. This normalization is used to compare samples in different environments and to be able to identify the molecular structures and changes between them. [26]. In the spectrum, nuclei absorbed in downfield (to the left) are the molecules with less shielding and require a lower field strength for resonance than those absorbed to the right.

Intensity
The intensity on the y – axis represents the concentration of nuclei or molecules observed in the sample, meaning a decrease in intensity corresponds to a decrease of the molecules studied [26]. The peak intensity shows the signal strength of the nuclei in the sample, for a quantitative analysis the peak areas are used as it reflects the number of nuclei in the environment [23].

Relaxation times
Relaxation time in NMR describes the phenomenon of nuclear spins returning to equilibrium after excitation by the radio frequency (RF) pulse. The nuclei spin possess magnetic moment along three orthogonal axis x, y and z [23]. In the presence of an external magnetic field B_0 the spins align along the z-axis, when an RF pulse is applied, the net magnetization is tilted into the x-y plane where it can be detected as signal [26].

Longitudinal relaxation (T_1) describes the recovery of magnetization of the z-axis after excitation, which comes from the energy exchange between the nuclear spins and molecular environment [26]. T_1 is defined as the time it takes the longitudinal magnetization to recover 63 % of the equilibrium value [27]. Inversion recovery (IR) sequence is often used to measure T_1, by applying a 180° inversion pulsed followed by a delay and a 90° excitation pulse [26], the delay time is varied. Saturation recovery is another method for T_1 measurements which is faster but less accurate. Repeated RF pulses are applied with short repetition time (TR) getting the longitudinal magnetization close to zero [27]. To be able to record the signal a 90° pulse is applied.

Transverse relaxation (T_2) describes the decay of magnetization in the x-y plane [26]. The spins initially rotate together but after excitation they interact with each other in phase and slowly the signal in the x-y plane disperses. The time it takes for transverse magnetization to decay 37 % of its initial value is the T_2 or transverse relaxation time [27]. In NMR, T_1 and T_2 relaxation times provide information about molecular mobility, intermolecular interactions, and structural heterogeneity of the sample [26].

The spin echo (SE) sequence is used to measure true T_2 by refocusing the magnetization [28] by first applying 90° excitation pulse followed by a 180° to compensate for field inhomogeneities. Further improvement of the T_2 value can be achieved by applying multiple 180° pulses to produce a train of echos by the Carr–Purcell–Meiboom–Gill (CPMG) sequence [29]. Two important parameters are echo times (TE) and repetition time (TR) for these measurements. TE is the time between initial 90° pulse and the echo determines the extent of T_2 decay [27]. TR is the time between successive pulse sequences and controls the degree of T_1 recovery.

Diffusion
NMR can also be used to study diffusion which is the random movement of the molecules in a sample [26]. Diffusion is measured by applying magnetic field gradients which makes the nuclear spins position dependent. The molecular mobility and structure is observed by the phase changes of the molecules which gives a measurable signal [27].

2.5.1 ^{1}H NMR

Studying organic compounds ^{1}H NMR is the preferred method. ^{1}H NMR uses the hydrogen nuclei to give the spectrum [23]. Hydrogen is of abundance in biological and organic matter. Fats, proteins and carbohydrates are all types of matter that fall into these categories and easily be detectable by ^{1}H NMR.

2.5.2 Low-Field NMR

Low field NMR uses a much lower magnetic field strength for its experiments compared to high field NMR. The usage of lower magnetic field makes it cheaper and more compact but it also lowers the spectral resolution [30]. It is of great use in applications where molecular structure is not of as big importance such as studying relaxation times and in fields like food science and polymers. These properties make it suitable to use in industrial processes and for routine analysis.

2.5.3 Time Dependent Nuclear Magnetic Resonance (TD-NMR)

TD-NMR uses NMR theory to solely focus on relaxation times of the sample [5]. It therefore does not provide a full chemical spectrum as ^{1}H NMR, but the advantage is the much faster processing time when chemical spectrum is not needed. It's ease of use and possibility to be used with an auto sampler is why it is used in many industries for in-line usage [5]. A lower field strength is also often used with TD-NMR.

2.5.4 Magnetic Resonance Imaging (MRI)

MRI is an imaging technique based on the principles of NMR that yields spatially-resolved maps of MR observables. These maps are used to visualize structures, phase behaviours and homogeneity in systems [27]. It is also able to provide information about stability and effects of processing or time variables. MRI is similarly to NMR non-destructive with low sensitivity [31].

Differences in T_1 and T_2 are used in MRI to obtain image contrast since they are sensitive to different properties. Longitudinal relaxation (T_1) is sensitive to molecular mobility and T_1-weighted images provide information about the composition of the sample [27]. Transverse relaxation (T_2) is sensitive to structural heterogeneity and molecular mobility, T_2-weighted images provides information about the structural features of the sample [27].

The relaxation processes are observed with similar pulse sequences used in NMR to extract the wanted information. The spin echo sequence is used in MRI with Multi-slice multi-echo (MSME). This enables faster and more efficient T_2 mapping [27] by taking multiple echos and slices in one experiment and it highlights where structure or mobility differs.

Inversion recovery in MRI provides information about T_1 and molecular dynamics and interactions. Combining these two relaxation times provides complementary information about both interactions and structural changes in the sample while also identifying and localizing contaminants non-destructively.

2.6 Exponential and Distribution Based Models for Data Fitting Models

The complexity of milk and the changes in its behaviour during spoilage needs the implementation of different mathematical models to be described. The models used were mono-exponential, bi-exponential, stretched exponential and gamma distribution-based. With the ability of all four models the complexity in milk can be explained from the simple processes to the heterogeneous parts where single-parameter behaviour may not be justified.

2.6.1 Mono-Exponential Model

A system described by a single relaxation time where it assumes uniformity through the whole system. Mono-exponential models are often preferred at early stages for understanding and also are preferred in a homogeneous system [32]. The model is explained by 2.3 where A is the amplitude, τ the characteristic relaxation time and C represents the constant offset for background noise.

$$y(t) = Ae^{-t/\tau} + C \tag{2.3}$$

2.6.2 Bi-Exponential Model

A more complex system where two processes are present simultaneously and two relaxation times could be observed. The bi-exponential model is used for systems where data suggest the multiple processes are found, such as a heterogeneous system. The model is explained by 2.4 where A is the amplitude, τ the characteristic relaxation time and C represents the constant offset for background noise.

$$y(t) = A_1e^{-t/\tau_1} + A_2e^{-t/\tau_2} + C \tag{2.4}$$

2.6.3 Stretched Exponential Model

The stretched exponential model is used for a system with a distribution of relaxation times rather than a set and is used to identify if there is a need for a bi-exponential model. It is often used for systems with multiple motions or components and where simple exponential decay deviations are observed [33]. The model is explained by 2.5 where A is the amplitude, τ the characteristic relaxation time, β the stretching component and C represents the constant offset for background noise.

$$y(t) = Ae^{-(t/\tau)^{\beta}} + C \tag{2.5}$$

2.6.4 Gamma Distribution Model

The gamma model is able to describe the system as continuous distribution of exponential processes [34]. When relaxation processes are overlapping it provides a more realistic and flexible interpretation from the data. The model is explained by 2.6 where A is the amplitude, τ the characteristic relaxation time, k the shape parameter, θ scaling parameter, $\Gamma(k)$ the gamma function and C represents the constant offset for background noise.

$$y(t) = A\frac{t^{k-1}e^{-t/\theta}}{\theta^k\Gamma(k)} + C \tag{2.6}$$

2.6.5 Model Evaluation Metrics

To assess the quality of the fitted models for the given data several metrics were used to compare between the models. These were used to evaluate how well the model describes the data and if its usage induced unnecessary complexity and decrease the stability.

R^2 explains the portion of the variance in the data explained by the model, ranging from 0 for a bad fit to 1 for a perfect fit but does not penalize complexity and therefore often favours overfitting. RMSE measures the average difference between predicted and real values and provides fitting prediction in absolute terms, where a lower value indicates better fit. Akaike Information Criterion (AIC) and Bayesian Information Criterion (BIC) both evaluate the models by balancing the complexity and goodness of fit [35]. They both penalize unnecessary parameters usage where BIC favours simple models with higher penalties than AIC for unnecessary parameters. A lower value for AIC and BIC indicates a better model.

3
Methods

This section will present the methods and instruments used for analysing milk spoilage. Further, the section also covers how the data from the experiments were evaluated and analysed.

3.1 Sample Preparation

Three microorganisms (*Leuconostoc mesenteroides, Exiguobacterium undae*, and *Pseudomonas chlororaphis*) were used in this study. Each microorganism was introduced separately into sterile Milbona 3.5 % UHT milk under sterile conditions following a standard of Tetra Pak method.

1.7 ml of the incubated milk were transferred into 5 mm NMR tubes and 35 ml in 40 mm Falcon tubes which were sterilized prior to usage. After preparation the samples were transported to Chalmers in a cold box to delay microbial growth and connected enzymatic activity to ensure a controlled starting point. Upon arrival at Chalmers, the samples were placed inside an incubation room set at 30°C and incubated for up to 8 days. From this stock samples were taken at different time points for measurement to determine the effect of microbial contamination on milk.

3.2 Preliminary study

Initial experiments were conducted to get baseline values from three different non-contaminated UHT milks with different fat and lactose contents. Arla 1.5 %, Arla 3% and Arla lactose free 1.5% were pipetted into sterilized 5 mm NMR tubes. These samples were analysed in the Magritek 60 MHz Spinsolve to obtain T_1 and T_2 for the different peaks associated with the components of interest (fat, lactose and water-dominated regions), and spectroscopy information. The Bruker minispec 20 MHz TD-NMR was used to obtain information about T_1 and T_2 at a lower magnetic field.

Instrumental stability was evaluated for both 20 MHz and 60 MHz with a contaminated sample run for five repeated measurements. These were intended to assess if inhomogeneities and experimental inconsistencies introduced errors in the ^{1}H - NMR results. All parameters from the preliminary study were kept for the remaining experiments on all instruments. The parameters are summarized in Tables 3.1–3.10.

3.3 Magnetic Resonance Measurements

Measurements were performed on two independently prepared sample sets at the same time points under identical experimental conditions. The first batch was conducted without replicates and the second one was done with two replicate samples. For the first batch the same samples were measured for each day, it was brought back into the incubation room after each experiment. For the second batch the samples who had been removed from the incubation room were discarded to help with continuous growth in the samples when tested, more similar to how an in-line process would work. The experiments were done for all three strains of microbes at Day 0, 1, 3, 6 and 8 after incubation.

3.3.1 MRI

MRI measurements were performed on a Bruker Avance 300 MHz with a 44 mm magnet. The contaminated samples in 40 mm Falcon tubes were removed from the incubation room and inserted into the MRI. With each new sample the probe was tuned and matched prior to measurements, all samples were placed at the same height for replicability. Diffusion data was obtained using diffusion tensor imaging, but diffusion was only measured for the first batch of samples as it did not provide any useful information about the contamination with the time constraint chosen. The diffusion parameters are shown in Table 3.1.

Table 3.1: Imaging parameters for diffusion-weighted MRI (DWI)

Parameter	**Value**
Sequence	DTiStandard
Repetition time (TR)	2000 ms
Echo time (TE)	19 ms
b-values	0–4750 s/mm^2
Diffusion direction	1
Number of experiments	5

T_1 relaxation times were obtained using a RARE sequence with variable repetition times (RARE-VTR). T_2 relaxation times were measured by using a multi slice multi echo pulse sequence (MSME). Parameters used for T_1 and T_2 are shown in Table 3.2 and 3.3. Further spectroscopic data were acquired using a single region PRESS sequence, water suppression, positioned to identify where differences in the sample could be seen. In Table 3.4 the parameters for the PRESS sequence can be seen.

Table 3.2: Imaging parameters for T_1 measurements using RARE

Parameter	Value
Sequence	RARE
Repetition times (TR)	850–15000 ms (10 values)
Echo time (TE)	5.02 ms
RARE factor	8
Number of averages	2
Number of repetitions	1

Table 3.3: Imaging parameters for T_2 measurements using MSME

Parameter	Value
Sequence	MSME
Repetition time (TR)	4891 ms
Echo times (TE)	10–320 ms (32 echoes)
Number of echoes	32
Number of averages	2
Number of repetitions	1

Table 3.4: Acquisition parameters for ^{1}H-MRS using PRESS

Parameter	Value
Sequence	PRESS
Repetition time (TR)	2500 ms
Echo time (TE)	20 ms
Number of averages	128
Voxel size	$3 \times 3 \times 3$ mm^3
Spectral bandwidth	4000 Hz
Data points	2048

Table 3.5: Common imaging geometry parameters for T_1, T_2 and diffusion MRI

Parameter	Value
Number of slices	15
Slice orientation	Sagittal
Field of view (FOV)	45×45 mm^2
Matrix size	128×64
In-plane resolution	0.352×0.703 mm^2
Slice thickness	1 mm
Slice gap	1 mm
Slice distance	2 mm

3.3.2 60 MHz NMR

^{1}H NMR experiments were performed on a Magritek Spinsolve 60 MHz to identify structural changes. This was done by combining the usage of spectroscopy with solvent suppression for the water peak using 1D PRESAT MULTI with the parameters shown in Table 3.6. The 5 mm NMR tubes were removed from the incubation room and directly inserted into the Spinsolve 60 to minimize temperature changes. The samples were, after the 1D PRESAT MULTI, measured for both T_1 and T_2 in accordance with the parameters shown in Table 3.7 and Table 3.8. For T_2 the usage of water suppression was also implemented by using a WET sequence rather than pressurization to minimize the effect on measurement.

Table 3.6: Shows the acquisition parameters used for obtaining the 1D - Presat Multi for Magritek Spinsolve 60

Parameter	Value
Scans	16
Acquisition time	3.2 s
Repetition time	15 s
Sat Power	-50 dB
Sat period	3 s

Table 3.7: Shows the acquisition parameters used for obtaining the T_1 for Magritek Spinsolve 60

Parameter	Value
Scans	2
Acquisition time	3.2 s
Repetition time	20 s
Max inversion time	15 s
Number of steps	9

Table 3.8: Shows the acquisition parameters used for obtaining the WET T_2 for Magritek Spinsolve 60

Parameter	Value
Correction factor	1
Dummy scans	2
Scans	8
Acquisition time	0.8 s
Repetition time	6 s
Number of steps	20
CPMG Echo time	0.5 ms
Final echo time	1 s

3.3.3 TD-NMR

A Bruker minispec mq20 was used for measuring T_1 and T_2 at a lower magnetic field strength of 20 MHz. The 5 mm NMR tubes with contaminated milk were after removal from the incubation room placed inside an 10 mm NMR tube. This was needed as the minispec only could facilitate 10 mm tubes and the samples were incubated in 5 mm tubes. T_1 was measured using the parameters shown in Table 3.9 using an inversion recovery experiment. T_2 was measured using a CPMG pulse sequence with the parameters shown in Table 3.10. Both experiments used multi-block acquisition, where the signal amplitude is recorded for each delay. To keep the measurements replicable the experiment's temperature was set to 30 °C, same as in the incubation room, to match the conditions.

Table 3.9: Shows the acquisition parameters used for obtaining the T_1 with Inversion recovery for Bruker minispec

Parameter	Value
Scans	8
Recycle Delay	1 s
Gain	60 dB

Table 3.10: Shows the acquisition parameters used for obtaining the T_2 with CPMG for Bruker minispec

Parameter	Value
Scans	32
Recycle Delay	4 s
Gain	81 dB

3.4 Penetration of Packaging

The effects of packing materials on signal penetration were investigated on the Bruker minispec mq20 TD-NMR. Two different packaging materials and one reference sample without packing material were evaluated. The packaging materials were a standard material and one material with an aluminium layer. The materials were wrapped around a 5 mm NMR tube of non-contaminated UHT milk and fastened with Teflon tape to minimize interference, where it was inserted into a 10 mm NMR tube for stability. For each material T_1 and T_2 were recorded with two replicates and the same settings were used as for earlier 20 MHz experiments in Table 3.9 and Table 3.10.

3.5 Data Analysis

The NMR and MRI results were processed using python and plotted to find trends. For the Magritek Spinsolve 60 data were extracted for three specific regions from integrals over different ppm regions in accordance with recommendations from the manufacturer [36]. The regions which were used for the Magritek Spinsolve 60 are shown in Table 3.11. The analysis focused on how the three different microorganisms affected the properties and structural changes in milk. This is shown with the help of evaluating relaxation times, spectrum and image based parameters from the different instruments used over time. The MRI and TD-NMR measures the bulk relaxation times and therefore no specific spectral regions were investigated with these techniques.

For obtaining T_1 and T_2 values, and being able to get slow and fast relaxation values, the data were investigated with four different fitting models to find the best option for each instrument and measurement. These models are mono-exponential, bi-exponential, stretched exponential and the gamma model. By applying all four models onto the experiments it was possible to detect which one provided the most stable and best fit for further investigation. The chosen model for each experiment setup was used for all stains and days for that given experiment setup.

The microorganisms were evaluated over eight days to identify changes over time and to connect relaxation times and spectroscopic information to get a full understanding of the spoilage effects. Differences obtained in relaxation times between different magnetic field strengths for the same sample were also investigated.

Table 3.11: Shows the ppm values of the regions of interest for the Magritek Spinsolve 60

Component	**Region (ppm)**
Fat	0.20 - 2.9
Lactose	2.90 - 3.86
Water	4.60 - 5.00
Water with others	2.80 - 7.00

4

Results and Discussion

Experiments were performed on two different batches. The first batch only contained one sample for each strain which was reused for all measurements over time, this provided information about how the microorganism growth changed in a single sample over time. This batch only observed how a single sample grew over time for each strain, but as microbial growth can vary largely between samples this did not reflect a real life situation. For an in-line process it should be possible to identify changes from spoilage even though only observing a sample once and not seeing its whole growth pattern. For the second batch several sample tubes were provided to study in a more similar way as an in-line process would. For each day two sample tubes were taken from the incubation room and tested as replicates for each strain, these samples were then discarded and for the next day new samples were used. This way of going about the experiment enabled to identify if all samples showed a similar trend over time with contamination or if it varied due to new samples every day. For the results the first batch will only be discussed for the first instrument of TD-NMR. Data and graphs for batch one for the other two instruments will be provided in the Appendix but not further discussed, this was done as they showed similar trends and the main batch of interest to enable an in-line process is the second one.

4.1 Baseline Measurements and Effects of Contamination on Relaxation Times

Baseline measurements were done with the Magritek Spinsolve 60 MHz as it enables to look at specific regions of the sample and investigate how these changes. The three different fat percentages showed how breakdown of fats would affect spectra and relaxation times, while the lactose free milk provided information about what changes could be seen when lactose is broken down.

The spectra from the four samples were overlaid in Figure 4.1 to observe the changes. In the lactose regions the three samples with lactose follow each other closely, while the lactose free milks significantly decrease over this region as well as introducing a new peak at 3.4 ppm. This peak is in the region of carbohydrates and could be the result of lactose hydrolysis which produces glucose and galactose. The differences in fat percentages can clearly be observed in the fat region where higher fat percentages produce larger peaks. The lactose content of the samples does not affect this region as observed by lactose free and regular milk with 1.5% fat showing similar peaks.

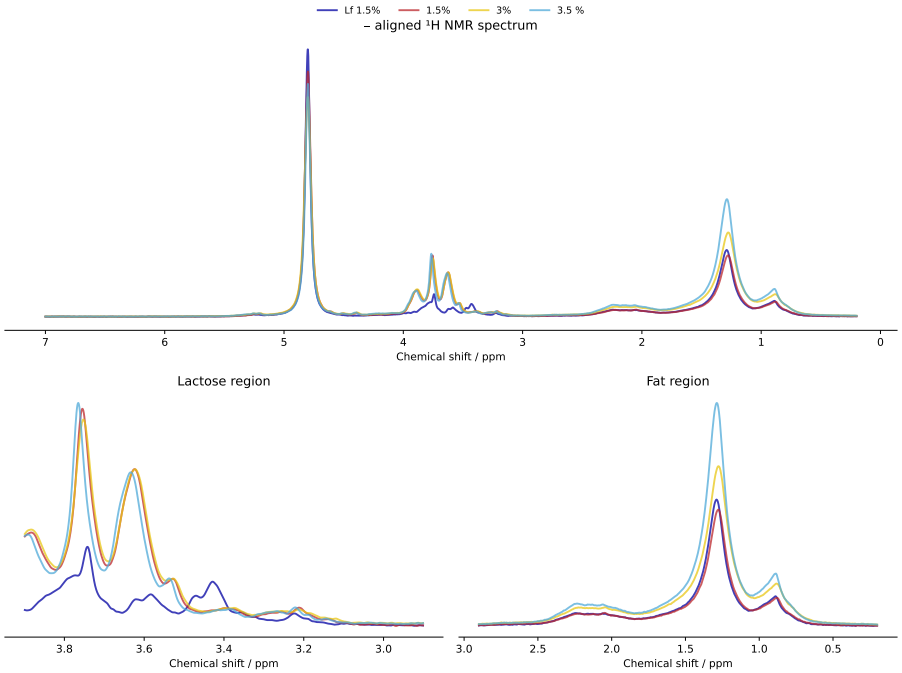

Figure 4.1: Illustrates aligned ^{1}H NMR spectra for four different samples with varying fat and lactose compositions. Lactose free Arla 1.5 % milk, Arla 1.5 %, Arla 3% and Milbona 3.5 %

Three regions were of interest for the relaxation times, these were chosen as they cover the area where contamination should show effect. The pure water region, a region at the water peak, was also chosen to see if this was influenced in any way. How the regions changed between samples are shown in Figure 4.2 and the data obtained is shown in Table 4.1. The relaxation times for the water-dominated region decreases from the lactose free to the standard milk where it is stable between fat percentages. This trend is also seen for the lactose region in T_2, which is expected given that the water-dominated region also encompasses a small part of the lactose region. T_1 for lactose does not show the same trend as it decreases with increasing fat content of standard milk. The increase of fat content reduces the molecular motion resulting in the observed decrease of T_1.

The increase of T_1 from lactose free to standard milk in the pure water region might be due to modified interactions going to glucose and galactose from lactose. The corresponding T_2 values only changes lightly due to a similar sample environment and it is less influenced by the changes from lactose hydrolysis. The fat region for T_2 stayed stable over all samples indicating fat percentages has low impact on T_2 relaxation of the fat region. This minimal change could be due to the fact that the region already was dominated by the local environment and change of the fat content in the sample did not have an effect on this. The increased fat content lowers fat's T_2 as seen in Figure 4.2, the lower T_2 for the lactose free milk could be a result of molecular dynamics from lactose hydrolysis.

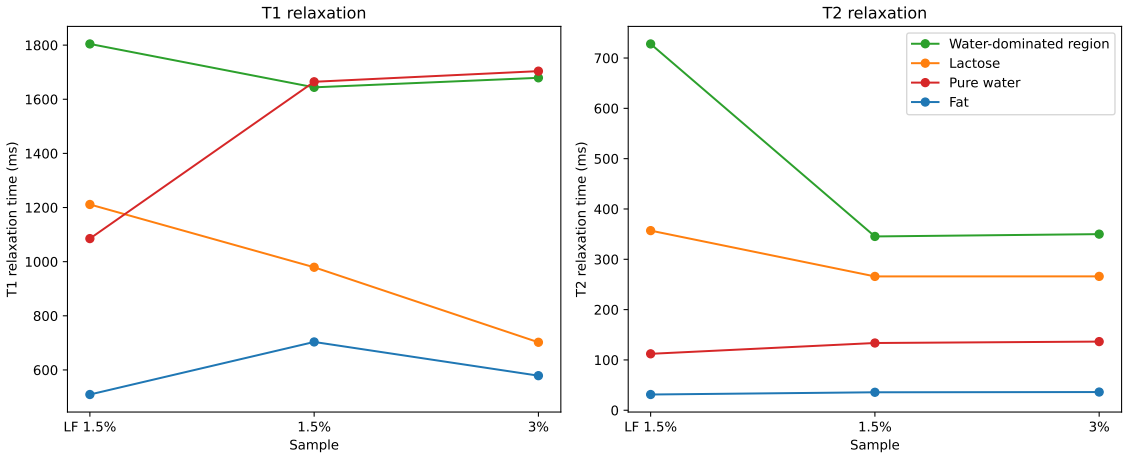

Figure 4.2: Illustrates four different samples with varying fat and lactose compositions. Lactose free Arla 1.5 % milk, Arla 1.5 %, Arla 3% and Milbona 3.5 %. It visualizes how T_1 and T_2 relaxation time change between them for the four regions.

Table 4.1: Baseline T_1 relaxation parameters and corresponding T_2 values measured at 60 MHz obtained with bi-exponential model.

		T_1 Parameters			T_2 Parameter
Sample	Region	$T_{1,1}$ (ms)	$T_{1,2}$ (ms)	Weighted T_1 (ms)	T_2 (ms)
Lf 1.5%	Fat	509.9	–	–	31.3
	Lactose	98.7	1644	1211.3	357
	Water-Dominated region	1804.4	–	–	728
	Pure water	1085.3	–	–	112.2
1.5%	Fat	703.4	–	–	35.7
	Lactose	343	2344	979.3	266.0
	Water-Dominated region	1644.0	–	–	345.4
	Pure water	1664.6	–	–	133.6
3%	Fat	578.8	–	–	36.2
	Lactose	69.5	2199.8	702.2	266.1
	Water-Dominated region	1679.2	–	–	350
	Pure water	1703.8	–	–	136.5

4.2 Low-Field TD-NMR (20 MHz)

The following sections presents and discusses the results obtained by using the 20 MHz TD-NMR. The graphs illustrate the overall trends differences between samples while the tables provide the corresponding numerical values.

4.2.1 Data Processing and Fitting

The recovery curves did not fully reach the long time plateau within the measured time range. S_∞ was fitted as a free parameter, as a result the obtained T_1 values are compared between samples rather than absolute relaxation values. Relative day-to-day comparisons are considered valid despite systematic uncertainty as they are the same over all samples.

All fitting models were evaluated, the more complex models produced lower AIC/BIC, however these models produced a short component at the lower boundary. This suggests an overfitting which is in line with the measurement not reaching the plateau. The mono-exponential model was selected as the model as it provided a stable and interpretable description for T_1.

The same problem could be seen in T_2 fitting models where bi-exponential provided weak separation of components and one of the components was close to the imposed boundary. The stretched model yielded a β close to 1 indicating mono-exponential behaviour over bi-exponential. More complex models all converged to the same value without providing more information. Therefore T_2 was also evaluated using a mono-exponential model.

4.2.2 Relaxation times

The first batch was evaluated at 20 MHz, the data from each organism are visualized in Figure 4.3. The second batch is visualized in Figure 4.4 where the mean is shown with error bars representing the standard deviation in the two replicates. *E. undae* and *L. mesenteroides* show a slight increase of T_2 over time in batch 1 from 160 ms to 170 ms. This trend is not seen in batch 2 where both of these are slightly decreasing, *E. undae* more than *L. mesenteroides*, from a starting point of 177 ms. For batch 2 *E. undae* also have a large standard deviation for day 6 for T_2. The other strains all show low standard deviation over time for T_2 indicating that the observed trends are a trend of the organism behaviour and a decrease in T_2 could represent a presence of contamination. *P. chlororaphis* for both batches shows a downward trend over time.

T_1 shows larger discrepancies in the measured values. *L. mesenteroides* indicate an increasing value over time for both batches, however large standard deviation in day 6 and 8 for batch 2 results in that no clear trend can be seen. This could also indicate that the microorganism impacts the relaxation time in different ways, and after longer times these start to vary from sample to sample due to that microbial growth is not linear. *P. chlororaphis* also shows these large differences for day 3 and 8, further indicating how complex milk is as a system and also how many different things could affect the relaxation time. The overall trends of T_1 for each microorganism are hard to distinguish where for batch 2 a slight increase from day 0 to day 8 was observed. This is not seen in batch 1 where the T_1 goes both up and down, however nearly all the values for batch 1 do fall into the error bars of batch 2. This indicates that both batch 1 and 2 values are present in the same deviation and the large standard deviations seen are possibly due to different mechanisms present from the microorganisms.

The larger discrepancies seen in T_1 could be related to how T_1 is more affected by changes in the chemical environment such as organic contaminations. Contaminations do alter the chemical environment due to protein breakdown, water mobility and more. These factors can vary substantially between samples and growth times causing T_1 to have larger deviations than T_2. The overall structure of the milk stays more stable even after introducing contaminations, this is what mainly affects T_2 and therefore smaller deviations are observed.

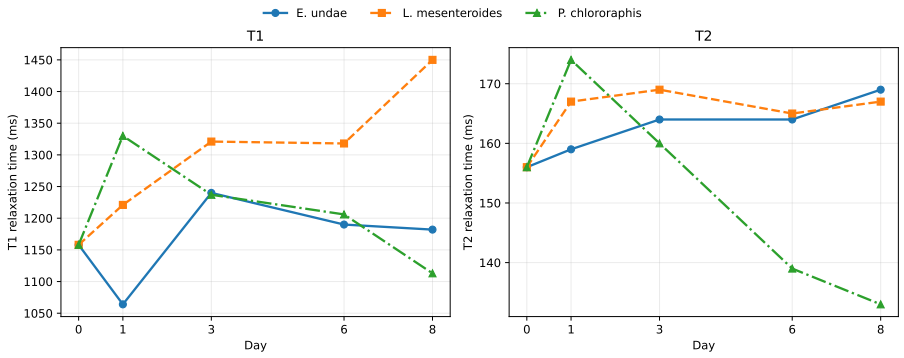

Figure 4.3: Changes in T_1 and T_2 relaxation times over 8 days *for E. undae, L. mesenteroides*, and *P. chlororaphis* for batch 1 measured at 20 MHz.

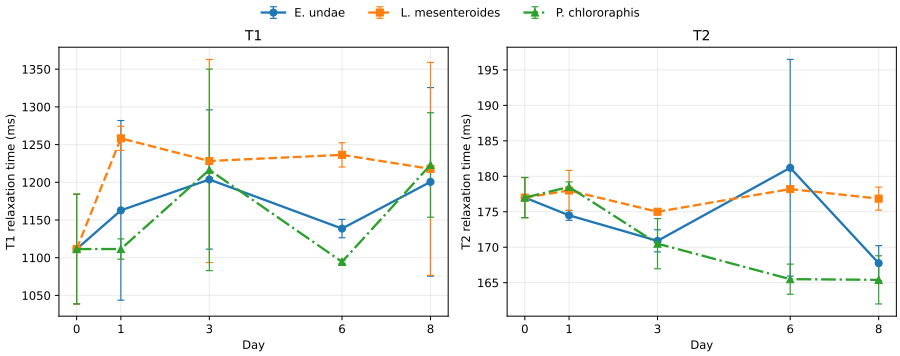

Figure 4.4: Mean T_1 and T_2 relaxation times (n = 2, mean ± SD) over 8 days for *E. undae, L. mesenteroides*, and *P. chlororaphis* for batch 2 measured at 20 MHz.

In Tables 4.2 and 4.3 the numerical values from both batches are shown. Here the same trends can be observed but more easily compared with exact values for mean and standard deviations to confirm the trends identified in Figure 4.3 and Figure 4.4. All measured values are all summarized in Appendix C.

Table 4.2: Relaxation times measured for batch 1 at 20 MHz.

Strain	**Day**	T_1 **(ms)**	T_2 **(ms)**
E	0	1158	156
E	1	1064	159
E	3	1240	164
E	6	1190	164
E	8	1182	169
L	0	1158	156
L	1	1221	167
L	3	1321	169
L	6	1318	165
L	8	1450	167
P	0	1158	156
P	1	1330	174
P	3	1237	160
P	6	1206	139
P	8	1113	133

Table 4.3: Relaxation times for batch 2 at 20 MHz presented as mean ± standard deviation from two replicates.

Strain	**Day**	T_1 **(ms)**	T_2 **(ms)**
E	0	1111.5 ± 72.8	177.0 ± 2.8
E	1	1162.8 ± 119.1	174.5 ± 0.7
E	3	1203.7 ± 92.3	170.9 ± 1.6
E	6	1138.6 ± 12.2	181.2 ± 15.3
E	8	1200.6 ± 125.1	167.8 ± 2.5
L	0	1111.5 ± 72.8	177.0 ± 2.8
L	1	1258.3 ± 16.0	178.0 ± 2.8
L	3	1228.2 ± 134.7	175.0 ± 0.0
L	6	1236.4 ± 16.1	178.2 ± 0.3
L	8	1217.9 ± 141.2	176.9 ± 1.6
P	0	1111.5 ± 72.8	177.0 ± 2.8
P	1	1111.5 ± 13.4	178.5 ± 0.7
P	3	1216.5 ± 133.6	170.5 ± 3.5
P	6	1094.5 ± 2.1	165.5 ± 2.1
P	8	1223.0 ± 69.3	165.4 ± 3.4

4.3 Low-Field NMR (60 MHz)

The following sections presents and discusses the results obtained by using the Magritek Spinsolve 60 MHz. The graphs illustrates the overall trends differences between samples in three different regions of interest, while the tables provides the corresponding numerical values. Spectra for the regions for each microorganism are also presented and discussed.

4.3.1 Data Processing and Fitting

The 60 MHz data was obtained by integrating over the regions of interest, the raw data was inspected for outliers which were removed before fitting. For fat T_1 was evaluated using a mono-exponential model, it provided a very good fit and close to ideal inversion. Bi-exponential provided a small second fraction of the signal, it was too small to be used and was attributed to overfitting. T_2 showed both mono- and bi-exponential environments across samples, therefore the stretched model was used as it captures the heterogeneity of the system without forcing the signal into two distinct components.

Lactose showed two distinct different environments in the system and the bi-exponential model was used for T_1. The T_2 for lactose showed clear mono-exponential in the raw data which was further strengthened by a β from the stretched model close to 1. The bi-exponential for T_2 and lactose improved AIC slightly but the second relaxation time was small and the raw data for lactose and T_2 showed clear mono-exponential behaviour and was therefore used.

T_2 for the water-dominant region provided a clear mono-exponential model with no detectable evidence of multi component relaxation behaviour or distribution. However for T_1 the water-dominant region showed a small fast relaxing component that may reflect contamination effects. The raw data supported that two components may be present, these components were observed as indicators of minor heterogeneity as the large water peak could hide the other relaxation times. The stretched model showed the best fitting with both fit quality and physical reliability as it had the most smooth behaviour over time. The bi-exponential fitting showed instability over time suggesting overfitting.

4.3.2 Spectra

Spectra were recorded for the three microorganisms over 8 days with the Magritek Spinsolve 60 MHz. Representative spectra for the three different microorganisms strains are shown in Figures 4.5–4.7. Spectra for two more batches for each microorganisms were recorded and is shown in Appendix D. For all spectra a decrease over time in the water peak was observed which can be related to changes in chemical environment, this include pH changes and increased interactions between water and other molecules resulting in reduced molecular motion. The lactose and fat regions show smaller differences over time for all microorganisms. The changes seen in the spectra are from different microbial activity depending on the microorganism.

Small changes in the NMR spectra are seen for *E. undae*. These could be the result of acid production at low level and the breakdown of casein to smaller peptides often seen for *E. undae* by proteolytic degradation. *P. chlororaphis* has the least active mechanisms but similar to *E. undae* it has proteolytic degradation, it also could affect the spectra by lipases activity which releases volatilize fatty acids altering the lipid environment. For *L. mesenteroides* the changes are related to carbohydrate metabolization producing organic acids from breaking down lactose to lactic acid and acetate. In all samples changes in the water peak can be observed which could be due to changes in the environment and molecular mobility. For *L. mesenteroides* specifically this could also be related to the pH drop from acid production which could change the observed water peak and also lead to aggregation of casein micelles.

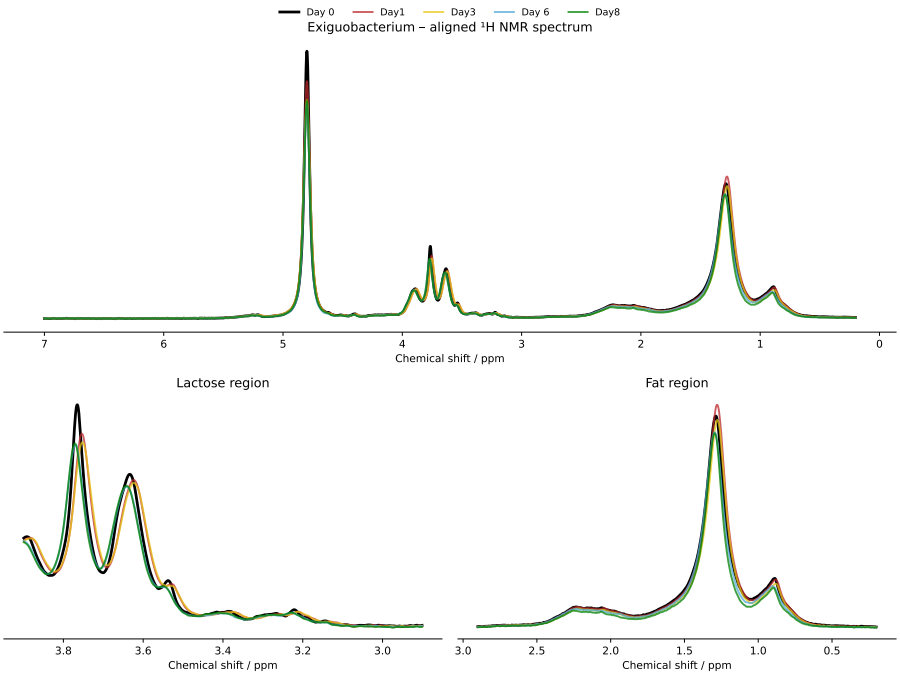

Figure 4.5: Aligned ^{1}H NMR spectra of *E. undae* samples collected over 8 days, highlighting changes in the lactose and fat regions

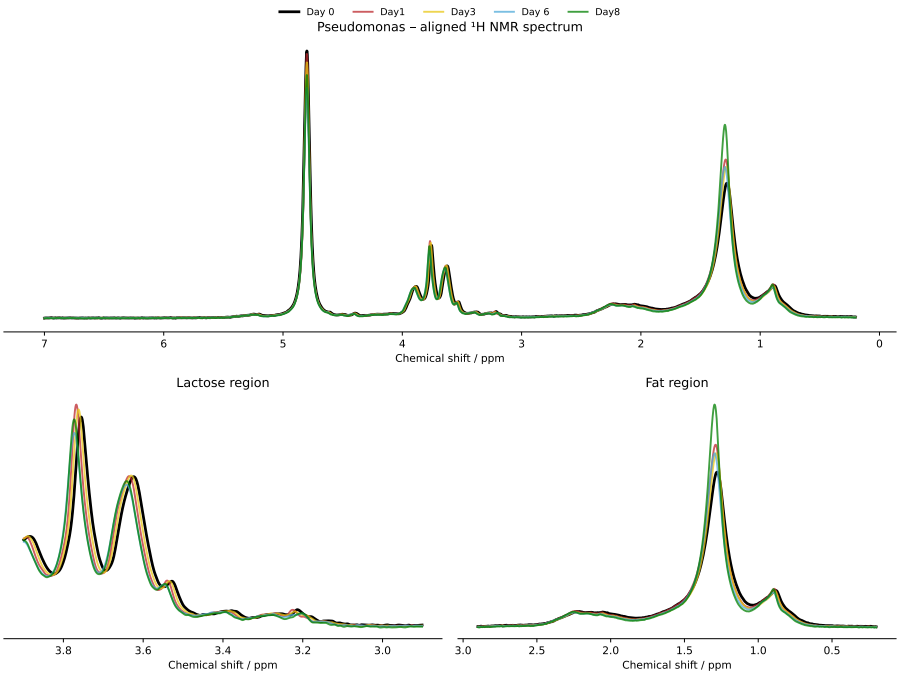

Figure 4.6: Aligned ^{1}H NMR spectra of *P. chlororaphis* samples collected over 8 days, highlighting changes in the lactose and fat regions

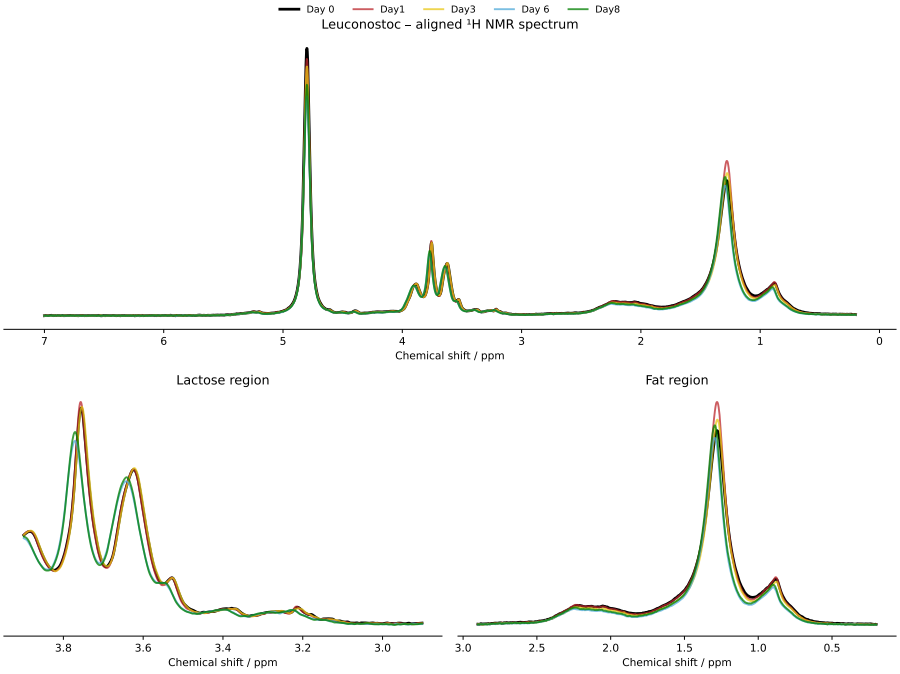

Figure 4.7: Aligned ^{1}H NMR spectra of *L. mesenteroides* samples collected over 8 days, highlighting changes in the lactose and fat regions

4.3.3 Relaxation Times

Relaxation times for the fat region in the samples are demonstrated in Figure 4.8. T_2 presents a slight increase from day 0 and stabilizes out, however the large deviations seen between the two replicates mean that a trend can not clearly be observed. The same can be said for T_1 where there also are no clear trends, with large deviations between days and increasing and decreasing T_1's from day to day as well. The unclear trends seen for fat could be related to the high degree of heterogeneity of fat in milk which can cause large discrepancies in molecular motion and measured relaxation times. This is also from the stretched fitting model used for the fat region because of its heterogeneity without uniform relation times. This model can lead to a broader distribution of relaxation values for the complex system studied leading to more unclear trends to be observed.

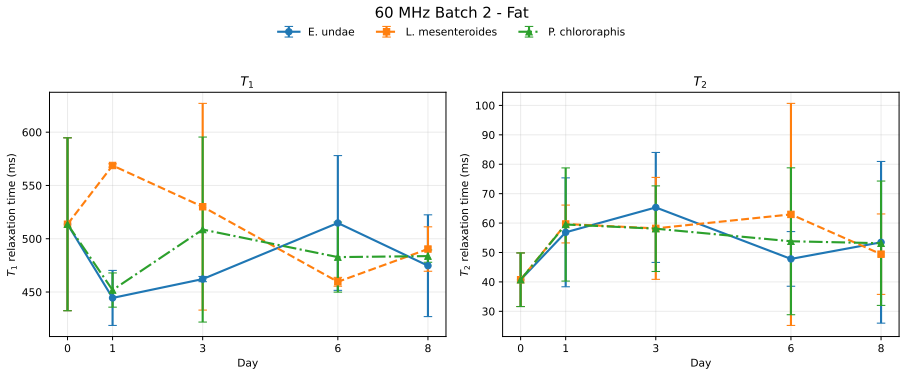

Figure 4.8: Mean T_1 and T_2 relaxation times (n = 2, mean ± SD) over 8 days for *E. undae, L. mesenteroides*, and *P. chlororaphis* for batch 2 measured at 60 MHz for the fat region

The shorter relaxation time for the lactose regions presented as $T_{1,1}$ in Figure 4.9 demonstrates a dipped curve for *P. chlororaphis* while both *E. undae* and *L. mesenteroides* demonstrates a more uniform and flat trend. *L. mesenteroides* at day 6 shows a small dip down but the large deviation makes it unclear how the trend changes for this day. For the longer relaxation time $T_{1,2}$ shows a slight increase from day 0 to day 8. Between these times the microorganisms behaviour differs, *L. mesenteroides* increases first until day 1 where it slowly decreases down to the final value at day 8. *E. undae* and *P. chlororaphis* respectively also follow this trend with an increase at first, and later a decrease back down to the same value at day 8. *P. chlororaphis* highest values are observed at day 3 and for *E. undae* this peak is reached later at day 6. All three microorganisms converge to the same value on day 8 and the largest deviation for them respectively are on the day where their peak values are observed indicating this peak behaviour might not be trend and instead a sample difference seen at these days.

The amplitude weighted T_1 combines both the shorter and longer T_1's, with their respective fractions, and follows more the longer relaxation times with an increased deviation for each day observed for *L. mesenteroides*. *E. undae* and *P. chlororaphis* presents nearly the same curve with a lowest point at day 1 increasing until day 6 where it stabilizes out for day 8. T_2 for *L. mesenteroides* shows a flat curve with low deviation indicting T_2 for the lactose region is not affected by *L. mesenteroides*. The T_2 for *P. chlororaphis* at day 3 and day 6 shows large deviations, the overall trend for them is a decrease over time. However by the large deviations this decrease could be an effect of sample differences, but at day 0 and day 8 the deviation is minimal indicating the decrease is viable but the trends between this can not easily be explained. Lastly *E. undae* also shows large deviations for T_2 on day 3 and day 8, the overall trend does imply minimal changes similar to *L. mesenteroides* for the lactose region. Possible a slight decrease for the middle times points of the experiment but the deviations makes it difficult to determine their true nature

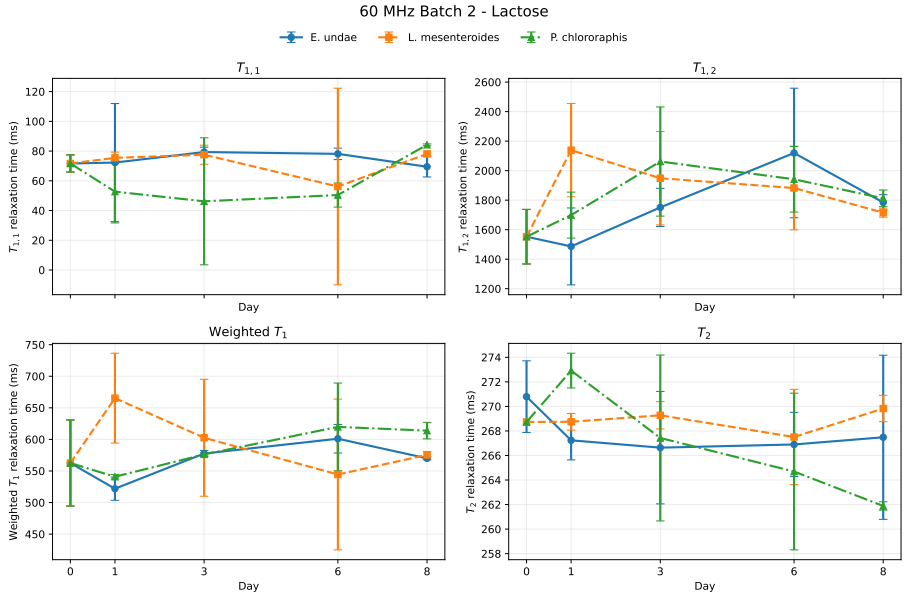

Figure 4.9: Mean $T_{1,1}$, $T_{1,2}$,weighted T_1 and T_2 relaxation times (n = 2, mean ± SD) over 8 days for *E. undae, L. mesenteroides*, and *P. chlororaphis* for batch 2 measured at 60 MHz for the lactose region.

The trend of T_1 for the water-dominated region of milk illustrated in Figure 4.10 shows a sharp trend upwards for all microorganisms with a slight reduction of strength for day 8. Low deviation for all days is observed indicating that contamination over time increases the T_1 for the water-dominated region. For T_2 any similar trends are hard to observe with the large deviations that are observed for day 6 and day 8 throughout. With the increasing and then decreasing trend trend observed for *P. chlororaphis* and *E. undae* with large deviations while *L. mesenteroides* is constantly stable indicates that the trend for T_2 could be stable with the large deviations coming from the differences in samples tested.

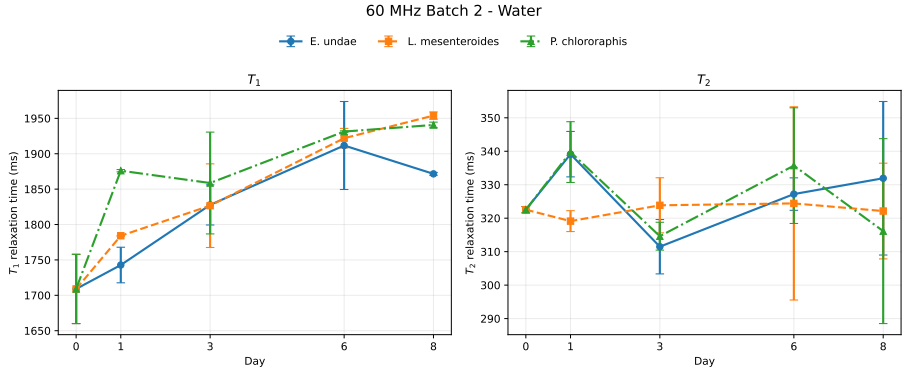

Figure 4.10: Mean T_1 and T_2 relaxation times (n = 2, mean ± SD) over 8 days for E. *undae, L. mesenteroides*, and *P. chlororaphis* for batch 2 measured at 60 MHz for the water-dominated region

In Table 4.4 the numerical values from batch 2 are shown. Here the same trends can be observed but more easily compared with exact values for mean and standard deviations to confirm the trends identified. The graphs and data for the regions from batch 1 are presented in Appendix D.

Table 4.4: Mean relaxation parameters measured at 60 MHz for batch 2 in the water-dominated, fat, and lactose regions. Values are reported as mean ± SD of replicate measurements.

Strain	Day	Water-dominated Region		Fat Region		Lactose Region			
		T_1 (ms)	T_2 (ms)	T_1 (ms)	T_2 (ms)	$T_{1,1}$ (ms)	$T_{1,2}$ (ms)	Weighted T_1 (ms)	T_2 (ms)
E	0	1709.0 ± 49.9	322.6 ± 0.5	513.6 ± 80.3	40.7 ± 9.1	71.7 ± 5.7	1652.3 ± 325.6	562.9 ± 68.9	272.7 ± 5.6
E	1	1763.9 ± 53.4	339.1 ± 3.4	444.3 ± 25.6	62.0 ± 10.7	72.6 ± 39.6	1619.0 ± 72.9	567.3 ± 20.0	267.7 ± 1.1
E	3	1823.7 ± 22.6	311.5 ± 8.4	462.3 ± 2.1	66.1 ± 17.6	79.6 ± 3.5	1723.1 ± 279.4	577.7 ± 5.1	265.9 ± 2.6
E	6	1890.8 ± 7.4	316.9 ± 10.1	515.9 ± 64.6	47.9 ± 9.7	74.3 ± 5.1	1840.2 ± 27.8	576.4 ± 22.4	265.9 ± 5.8
E	8	1870.5 ± 2.1	332.0 ± 23.5	474.6 ± 47.3	53.5 ± 27.5	69.7 ± 7.1	1781.2 ± 56.4	580.3 ± 15.7	267.5 ± 7.3
L	0	1709.0 ± 49.9	322.6 ± 0.5	513.6 ± 80.3	40.7 ± 9.1	71.7 ± 5.7	1652.3 ± 325.6	613.9 ± 4.5	269.0 ± 0.5
L	1	1786.7 ± 2.3	319.1 ± 1.6	633.2 ± 92.4	59.7 ± 6.3	72.9 ± 1.2	2798.6 ± 796.8	692.8 ± 32.9	267.6 ± 1.9
L	3	1826.7 ± 59.0	324.3 ± 8.8	532.9 ± 99.2	58.0 ± 18.3	50.0 ± 46.5	1990.4 ± 1140.9	611.8 ± 79.9	268.8 ± 1.0
L	6	1918.4 ± 2.3	317.2 ± 18.2	461.6 ± 5.8	62.5 ± 37.0	56.8 ± 48.1	1418.7 ± 871.2	589.0 ± 49.4	270.8 ± 0.7
L	8	1953.1 ± 6.3	322.4 ± 14.3	490.4 ± 21.0	49.0 ± 14.6	75.8 ± 4.9	1830.3 ± 217.9	678.7 ± 75.6	261.1 ± 13.5
P	0	1709.0 ± 49.9	322.6 ± 0.5	513.6 ± 80.3	40.7 ± 9.1	71.7 ± 5.7	1652.3 ± 325.6	609.1 ± 2.4	273.6 ± 0.5
P	1	1812.7 ± 88.5	340.6 ± 5.4	451.7 ± 8.3	74.1 ± 0.7	72.1 ± 1.5	1694.3 ± 430.7	538.8 ± 6.3	270.6 ± 1.7
P	3	1858.7 ± 74.7	314.6 ± 2.3	506.2 ± 90.3	58.1 ± 16.0	38.0 ± 54.1	1642.1 ± 249.2	572.7 ± 7.3	267.5 ± 6.5
P	6	1932.2 ± 1.7	328.7 ± 6.3	482.7 ± 32.1	54.9 ± 24.0	50.7 ± 8.8	1981.7 ± 410.6	619.7 ± 69.6	264.6 ± 6.7
P	8	1950.7 ± 9.6	326.2 ± 42.5	483.8 ± 11.6	53.6 ± 20.5	76.6 ± 15.3	1737.2 ± 331.5	615.4 ± 14.4	261.9 ± 0.4

4.4 High-Field MRI Findings (300 MHz)

The following sections presents and discusses the results obtained by using the 300 MHz MRI. The graphs illustrates the overall trends differences between samples while the tables provides the corresponding numerical values.

4.4.1 Data Processing and Fitting

T_1 was fitted using a mono-exponential with offset, this accounts for baseline signal and retains a simple explanation of T_1. The model with and without offset produced similar values indicating model robustness with baseline treatment. The more complex models either collapsed to a single dominant parameter or lacked physical interpretation reaching bounds.

The T_2 data was best described by a mono-exponential mode, the bi-exponential model collapsed to a single dominant T_2 value and did not provide evidence for distinct relaxation populations. The stretched model further showed this with a β over 1 therefore not physically meaningful.

For diffusion a mono-exponential model was used due to the small amount of b-values recorded. The lower amount of values was only able to provide unstable or non-physical parameters. The mono-exponential was the most robust interpretable model.

4.4.2 Relaxation times

The relaxation times from the MRI is shown in Figure 4.11 where the error bars represent the standard deviation from the mean observed for batch 2. For T_1 all micrograms demonstrates an increase from day 0 to day 1 where they are more stable for the later days. *E. undae* demonstrates nearly having a perfect line with low deviation for the last three measurement times. For day 1 *E. undae*'s deviation is quite large but decrease significantly after. *L. mesenteroides* indicates a curved shape over time where a max is reached for day 3. After day 6, the T_1 dips down to the same value as on day 1. However the deviation shown for day 3 and day 6 indicates that the trend could be even more increasing from day 1 to day 8 for *L. mesenteroides*. For *P. chlororaphis* day 1 stands out with a large deviation in comparison with the other days. It shows a slight dip for day 3 but otherwise *P. chlororaphis* stabilizes with low deviation for the last measured times.

All microorganisms present the same trends for T_2 shown in Figure 4.11. At day 0 the same value was used as a reference point for all microorganisms, after this there is a sharp decrease in T_2 until day 1. For the three last measured times T_2 slowly builds back up with quite low deviation except for *E. undae* on day 6. The trend observed here, excluding the first data point, is an upward trend for T_2 from all microorganisms over the 8 days of incubation.

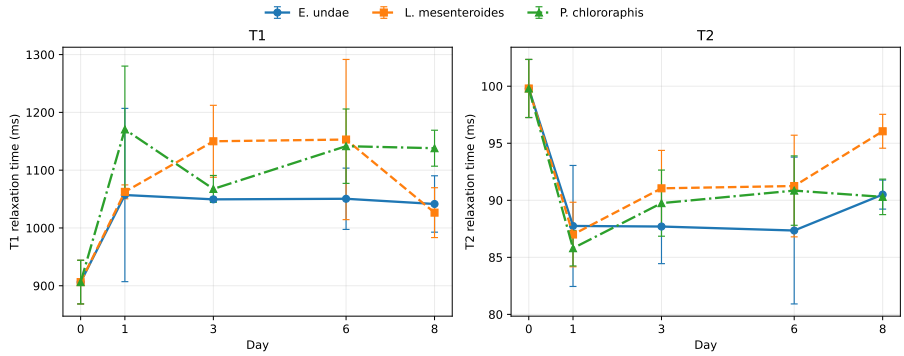

Figure 4.11: Mean T_1 and T_2 relaxation times (n = 2, mean ± SD) over 8 days for *E. undae, L. mesenteroides*, and *P. chlororaphis* for batch 2 measured at 300 MHz

In Table 4.5 the numerical values from batch 2 are shown. Here the same trends can be observed but more easily compared with exact values for mean and standard deviations to confirm the trends identified. The graph and data from batch 1 is shown in Appendix E.

Table 4.5: Relaxation times for batch 2 at 300 MHz presented as mean ± standard deviation from two replicates.

Strain	**Day**	T_1 **(ms)**	T_2 **(ms)**
E	0	906.3 ± 37.8	99.8 ± 2.5
E	1	1057.0 ± 149.9	87.8 ± 5.3
E	3	1049.5 ± 3.5	87.7 ± 3.3
E	6	1050.5 ± 53.0	87.4 ± 6.4
E	8	1041.5 ± 48.8	90.5 ± 1.3
L	0	906.3 ± 37.8	99.8 ± 2.5
L	1	1062.5 ± 12.0	87.0 ± 2.8
L	3	1150.0 ± 62.2	91.1 ± 3.3
L	6	1153.0 ± 138.6	91.3 ± 4.5
L	8	1026.5 ± 43.1	96.1 ± 1.5
P	0	906.3 ± 37.8	99.8 ± 2.5
P	1	1170.5 ± 109.6	85.8 ± 1.6
P	3	1067.5 ± 23.3	89.8 ± 2.9
P	6	1141.5 ± 64.3	90.9 ± 3.0
P	8	1138.0 ± 31.1	90.3 ± 1.6

4.4.3 Diffusion

For diffusion the apparent diffusion coefficient (ADC) remains approximately constant over time for all strains seen in Table 4.6 and Figure 4.12. Only minor fluctuations were observed which were within experimental uncertainty. With only having 5 b-values for extracting diffusion coefficients from these changes are neglectable. The error from noise or heterogeneity could influence the values more than what was seen. The time constraint involved together with earlier studies not showing differences from contamination with diffusion meant diffusion only was measured for the first batch and not perused for the later batch.

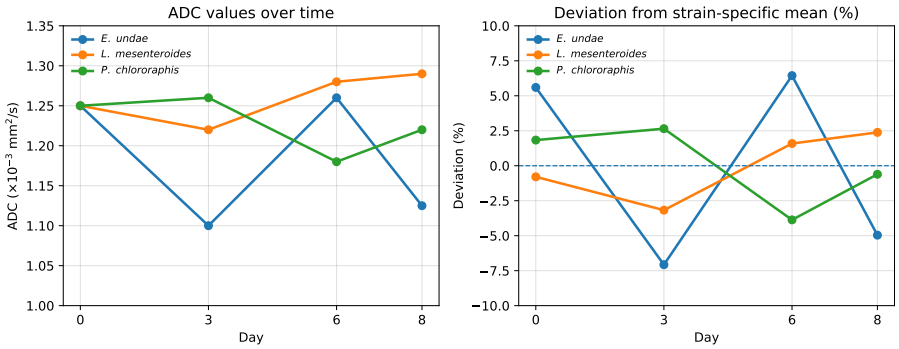

Figure 4.12: ADC diffusion over 8 days for *E. undae, L. mesenteroides*, and *P. chlororaphis* measured at 300 MHz

Table 4.6: Deviation of ADC from strain-specific mean ($\times 10^{-3}$ mm^2/s)

Strain	Day	ADC	Deviation	Deviation (%)
E	0	1.250	+0.066	+5.6
E	3	1.100	-0.084	-7.1
E	6	1.260	+0.076	+6.4
E	8	1.125	-0.059	-5.0
L	0	1.250	-0.010	-0.8
L	3	1.220	-0.040	-3.2
L	6	1.280	+0.020	+1.6
L	8	1.290	+0.030	+2.4
P	0	1.250	+0.022	+1.8
P	3	1.260	+0.032	+2.6
P	6	1.180	-0.048	-3.9
P	8	1.220	-0.008	-0.7

4.4.4 Homogeneity

The homogeneity of MRI samples were investigated to understand what differences in relaxation times could be observed depending on what part of the samples that were investigated. The Figures 4.13 - 4.15 shows how the samples distribution of T_2 relaxation times changes over incubation time and between microorganisms. All microorganisms show a decrease in largest T_2 value over time from the histogram, and the distribution becomes wider with time. The homogeneity of the samples were relatively good in the reference sample, over time more heterogeneity is observed for all samples.

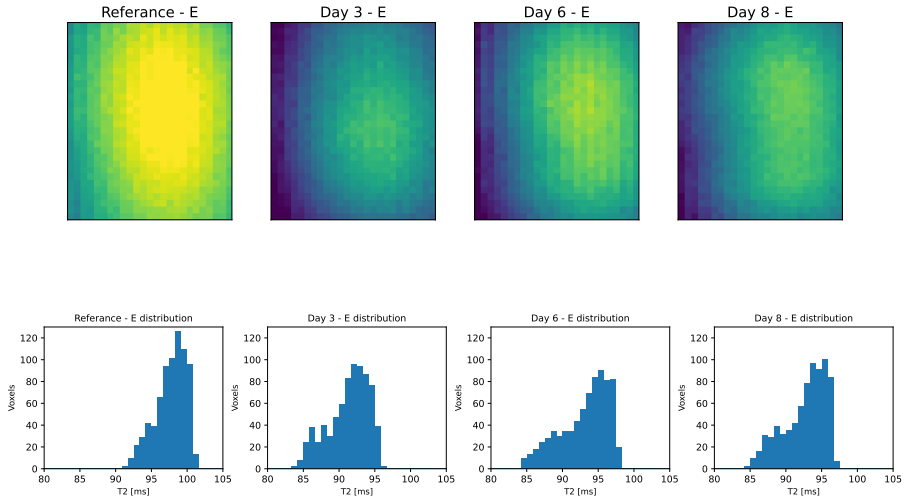

Figure 4.13: T_2 maps and corresponding T_2 values distributions for *E. undae* samples during 8 days of storage.

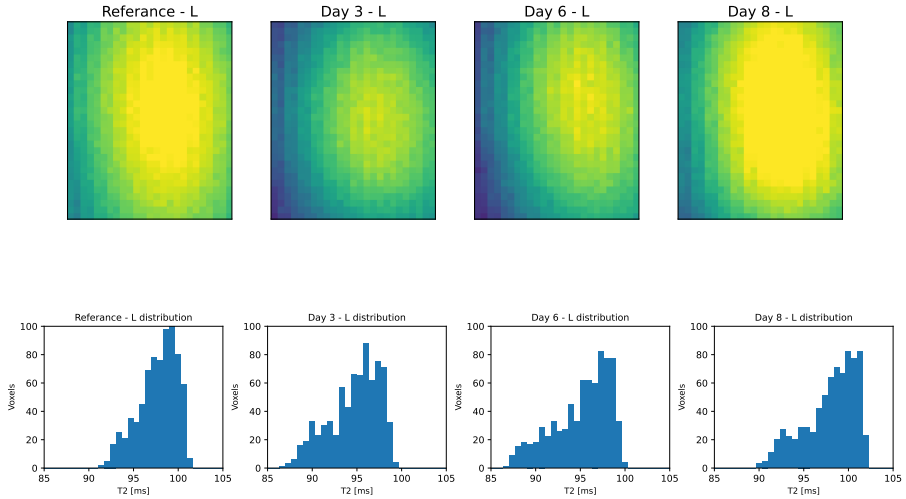

Figure 4.14: T_2 maps and corresponding T_2 values distributions for *L. mesenteroides* samples over 8 days of storage.

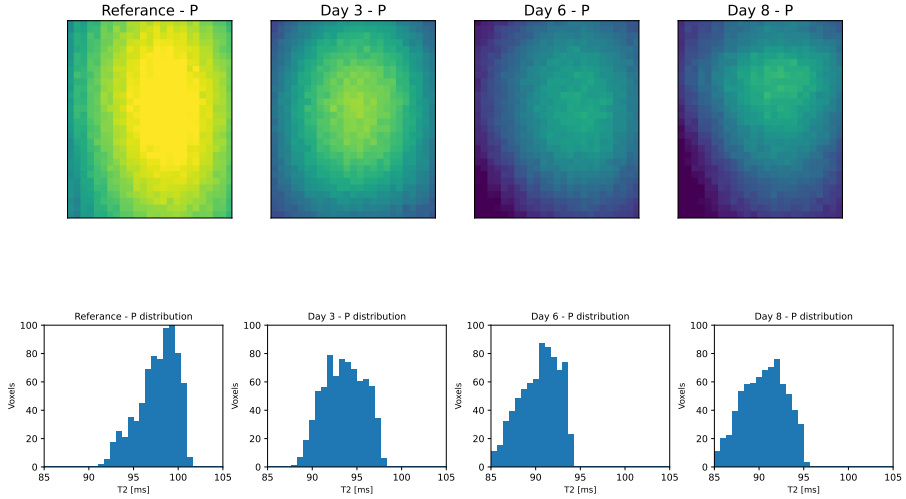

Figure 4.15: T_2 maps and corresponding T_2 values distributions for *P. chlororaphis* samples over 8 days of storage.

4.5 Comparison of Field Strengths

The three different instruments used varied in field strength from 20 MHz, 60 MHz and 300 MHz. Comparisons of the instruments were done by plotting the raw data shown in Figure 4.16 and Figure 4.17. From this, differences between the instruments could clearly be observed and an understanding of how the T_1 and T_2 from different instruments are related. In Figure 4.16 the curves for Spinsolve 60 MHz follow the same trend with different slopes. The MRI and TD-NMR 20 MHz deviated from the expected curve form. For the 20 MHz measurement this was due to experimental setup which did not fully allow the measurement to have a complete inversion recovery. The MRI starts off at a much larger value than the other instruments and this is due to the pulse sequence used for measurements. The saturation recovery pulse only detects positive recovery values.

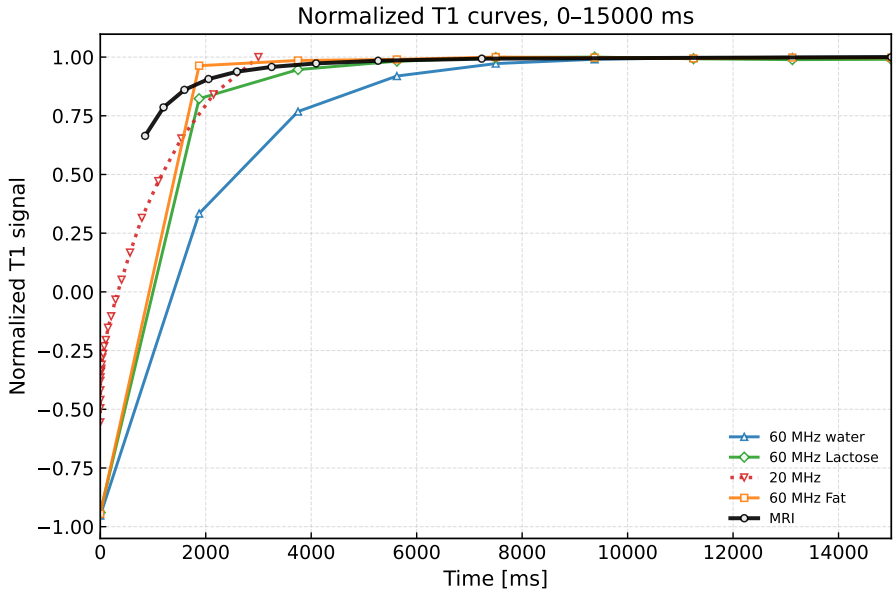

Figure 4.16: Normalized T_1 values compared for MRI, 60 MHz (water,fat and lactose) and 20 MHz

The T_2 curves in Figure 4.17 are more similar in shape. The curves for 60 MHz and 20 MHz follow each other well with straight lines with similar slopes, only the fat region stands out here with a faster decay linked to lipid chains having stronger interactions. The MRI shows the fastest decay that could be linked to the MSME sequence used which includes gradients and less pure measurement compared to CPMG used for the other instruments.

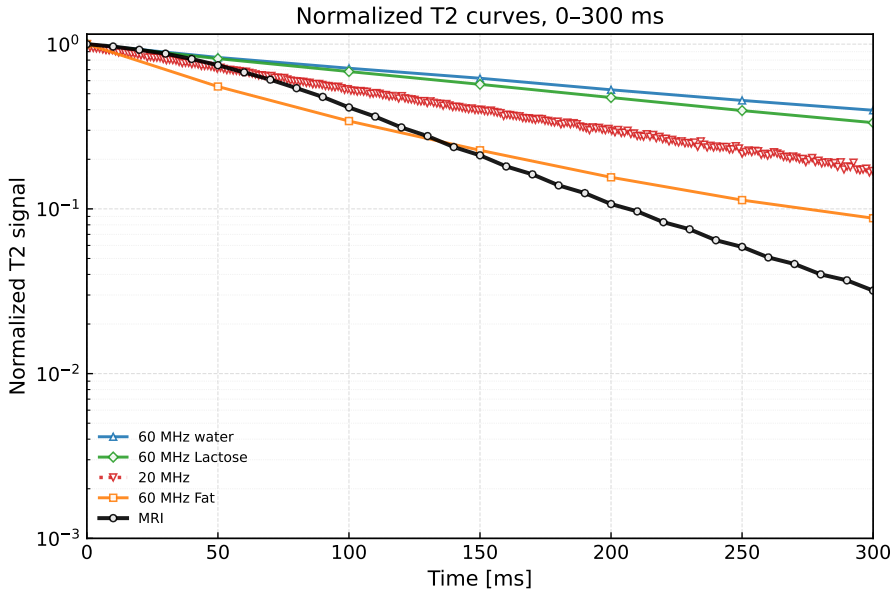

Figure 4.17: Normalized T_2 values compared for MRI, 60 MHz (water,fat and lactose) and 20 MHz

In Table 4.7 the mean values from batch 2 are calculated to make a comparison. The T_2 values measured at 20 MHz were constantly nearly double of the values measured at 300 MHz. This difference is probably linked to the different pulse sequences used for the MRI and TD-NMR but also due to lower dephasing effects at 20 MHz leading to increased T_2. For T_1 the differences in values between MRI and TD-NMR are not as large, this is because T_1 measurements are less sensitive to magnetic field inhomogeneities.

The Magritek Spinsolve 60 MHz measured relaxation times are fundamentally different as they are calculated for each region of interest therefore not directly comparable. Overall the differences between field strengths measurements provided complementary information about structure and mobility during storage. TD-NMR at 20 MHz represented bulk relaxation behaviour, at 60 MHz component specific relaxation times were observed and lastly at 300 MHz a higher magnetic field strength provided a comparison to low field measurements at 20 MHz.

Table 4.7: Comparison of relaxation times measured at 20 MHz, 60 MHz, and 300 MHz over storage time. The 60 MHz values are separated into water-dominated (W), fat (F), and lactose (L) regions. Values are averages of batch 2 replicates.

Strain	Day	20 MHz		60 MHz							300 MHz	
		T_1	T_2	W T_1	W T_2	F T_1	F T_2	L $T_{1,1}$	L $T_{1,2}$	L T_2	T_1	T_2
E	0	1111.5	177.0	1709.0	322.5	513.6	40.7	71.7	1652.3	270.8	906.3	99.8
E	1	1162.8	174.5	1742.8	339.1	444.5	56.9	72.3	1486.6	267.2	1057.0	87.8
E	3	1203.7	170.9	1827.7	311.5	462.1	65.3	79.4	1750.8	266.6	1049.5	87.7
E	6	1138.6	181.2	1911.6	327.2	514.8	47.8	78.1	2119.7	266.9	1050.5	87.4
E	8	1200.6	167.8	1871.6	331.9	474.7	53.5	69.5	1784.4	267.5	1041.5	90.5
L	0	1111.5	177.0	1709.0	322.5	513.6	40.7	71.7	1652.3	270.8	906.3	99.8
L	1	1258.3	178.0	1784.1	319.1	568.7	59.7	75.4	2138.8	268.7	1062.5	87.0
L	3	1228.2	175.0	1826.6	323.8	530.0	58.2	77.5	1948.5	268.3	1150.0	91.1
L	6	1236.4	178.2	1921.9	324.4	459.6	62.9	56.2	1882.2	267.5	1153.0	91.3
L	8	1217.9	176.9	1953.9	322.1	490.3	49.4	78.1	1715.1	269.8	1026.5	96.1
P	0	1111.5	177.0	1709.0	322.5	513.6	40.7	71.7	1652.3	270.8	906.3	99.8
P	1	1111.5	178.5	1876.0	339.8	451.8	59.5	52.7	1704.2	272.9	1170.5	85.8
P	3	1216.5	170.5	1858.6	314.6	508.6	58.3	46.2	2061.8	267.4	1067.5	89.8
P	6	1094.5	165.5	1931.3	335.7	482.8	53.8	50.4	1941.5	264.7	1141.5	90.9
P	8	1223.0	165.4	1940.7	316.1	483.7	53.6	84.2	1812.5	261.9	1138.0	90.3

4.6 Error for Reruns

To get an understanding of how much the data can vary in one single sample reruns were performed with a contaminated sample. The choice of a contaminated sample was done as it would show if layering or inhomogeneities from the contamination could affect the results from one single tube. The reruns were performed on the low-field instruments as these were the one of most interest for future research and industrial applications because of its lower cost and smaller size. MRI measurements were conducted, but additional reruns for error were not performed. In Figure 4.18 the spectrum in the Magritek Spinsolve was measured five times, here it is clear that the reruns produced identical spectra for each run. This indicates that differences observed between samples and days with spectroscopy shows how the sample changes its molecular structure or composition.

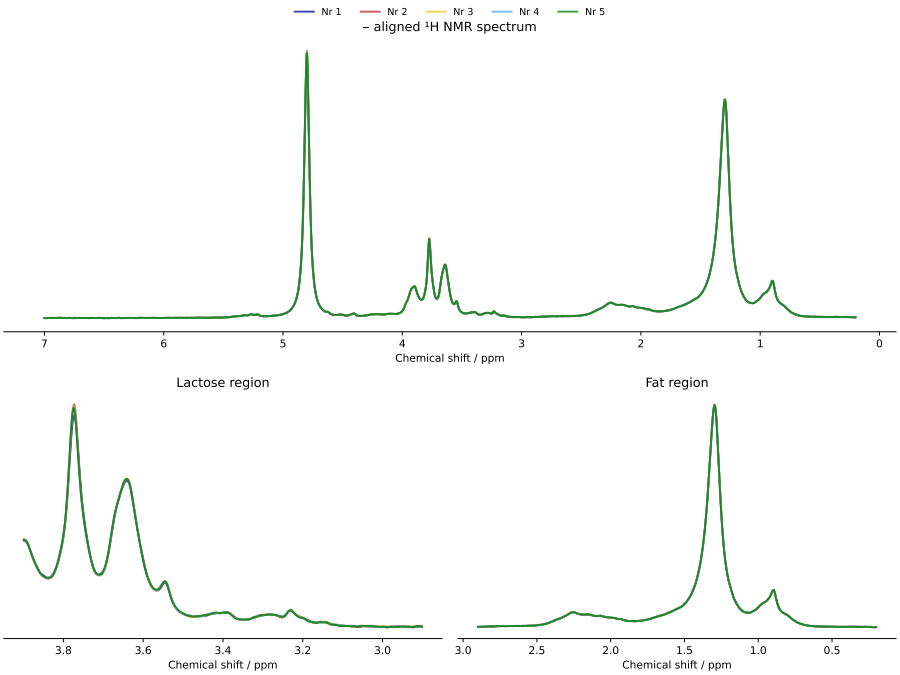

Figure 4.18: Five repeated spectra illustrating error for H-NMR in from Magrtiek Spinsolve 60

Further T_1 and T_2 were measured five times with both the Magritek Spinsolve 60 MHz and Bruker minispec 20 MHz. Figure 4.19 shows the data from the Bruker minispec and how the different reruns differed from the calculated mean. This was also done for the Magritek Spinsolve and these are presented in Appendix A. The means and SD from the instruments are summarized in Tables 4.8 and Table 4.9. In these tables it is possible to see how much a specific value could vary between samples, this helps with understanding what changes in relaxation times for the low-field instruments are significant.

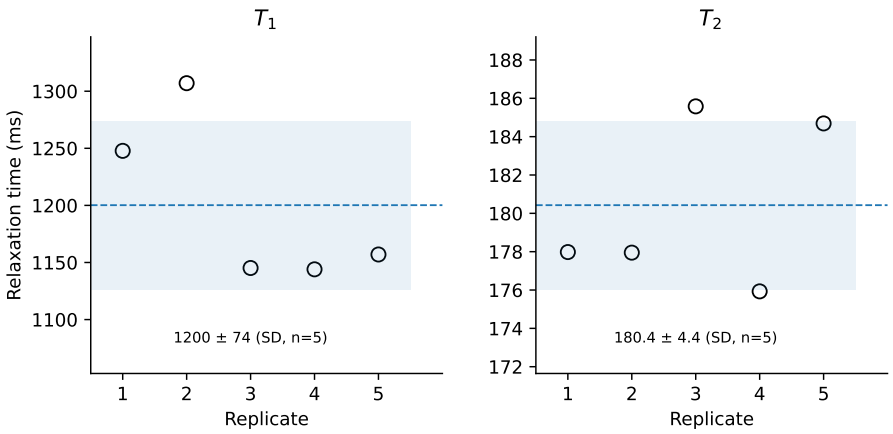

Figure 4.19: Five replicates measured at 20 MHz

Table 4.8: Summary of repeated relaxation time measurements at 20 MHz presented as mean ± standard deviation

Parameter	Mean ± SD (ms)	n
T_1	1200 ± 74	5
T_2	180.4 ± 4.4	5

Table 4.9: Summary of repeated relaxation time measurements at 60 MHz presented as mean ± standard deviation, separated into water-dominated, fat, and lactose regions.

Parameter	Mean ± SD (ms)	n
Fat region		
T_1	473 ± 11	5
T_2	82.6 ± 6.7	5
Lactose region		
Weighted T_1	616 ± 14	5
$T_{1,1}$	73.6 ± 23.6	5
$T_{1,2}$	2047 ± 66	5
T_2	268.1 ± 2.2	5
Water-dominated region		
T_1	1929 ± 4	5
T_2	306 ± 16	5

4.7 Overall Effects of Contamination on Measurements

This section discusses the changes seen from the microorganism over time. It further connects the observed changes to the theoretical background but also how these changes in the spectra, T_1 and T_2 are connected and explained by the use of different instruments and magnetic field strengths.

4.7.1 *Leuconostoc mesenteroides*

L. mesenteroides breakdown of lactose from carbohydrate metabolization to organic acids as lactic acid and acetate can be observed from the strong increase of T_1 in the water region at 60 MHz, from increased molecule mobility. The pH drop due to acid production can reduce the observed water peak over time which can be seen in the spectra for *L. mesenteroides*, indicating the acid production lowers the pH. The decrease of pH can also lead to aggregation of casein micelles contributing to observed changes in the spectra of the other regions as well.

At 60 MHz the fat region of *L. mesenteroides* shows larger fluctuations than the others suggesting larger heterogeneity of the region. T_2 at 20 MHz shows slight decrease for batch 2 and a slight increase for batch 1, whereas at 300 MHz the value first decreases from day 0 and slowly moves upwards. This combination of trends could be the results of structural rearrangements happening at different times depending on how the microorganisms grow. From this it could be emphasized how differently a microorganism can be interpreted over time, even though their microbial growth is similar it can depend on both time and placement of the sample. These changes are happening but at different times can be taken from the spectra where the fat and lactose regions are showing differences over time.

The increase seen in T_1 is consistently seen at both 20 MHz and 300 MHz. However the large standard deviation seen at some days obstructs a strong trend but it does further strengthen that rearrangements are showing at different days. And how relaxation times at specific days for the samples could vary largely.

4.7.2 *Exiguobacterium undae*

E. undae is demonstrating moderate and stable changes over incubation time for all magnetic field strengths. For T_1 a slight increase over time could be observed, whereas for the T_1 water fraction at 60 MHz shows a strong and clear increase over incubation time. This strong trend for the water region indicates water becomes more mobile over storage time as a result of proteolytic degradation, which from the theory should be seen for *E. undae*. The T_2 shows less strong trends with a slight decrease could be interpreted from the results.

The fat and lactose changes seen in the spectra and at 60 MHz further provides information that changes occurred. Even though the changes are small, the reruns of spectra suggest that any changes seen are from spoilage. This indicates that changes in lactose and fat regions have occurred, possibly from low acid production and breakdown of casein to smaller peptides. However from the stable T_2 the sample does not go through major breakdown, and a low increase of heterogeneity.

4.7.3 *Pseudomonas chlororaphis*

The least changes should be observed for *P. chlororaphis* due to its limited mechanisms. There should be proteolytic activity seen as breakdown of casein to peptides similar to *E. undae*. This could be related to the changes seen in the spectra where the water peak could be affected as well as the increased T_1 in the water region observed at 60 MHz. For *P. chlororaphis* an overall decrease over incubation time over all field strengths could be seen related to more restricted molecular motions or aggregation which could be a result of casein degradation.

The 60 MHz results further indicated a reduction of mobility and a more heterogeneous environment. All regions show reduced mobility over time with a decrease of T_2. For T_1 an initial increase is observed which stabilizes or decreases later on, this behaviour could be related to early structural changes in the sample and later in the heterogeneity of the system is increased.

The spectra show moderate changes in both fat and lactose regions, the changes in the lactose region are less pronounced. This could be related to how *P. chlororaphis* should not show breakdown of lactose and this behaviour could be linked to lipase activity which releases volatile fatty acids which can alter the lipid environment of the sample. The lipases activity could also explain the slight decrease in T_2 after day 1, related to more restricted molecular motion.

4.7.4 Overall Interpretation of Contamination Effects

Theoretically T_2 should be the most affected from milk spoilage due to its sensitivity to changes in molecular environments and heterogeneity of the sample. The microorganisms breakdown of lactose, proteins, lipids and carbohydrates can alter the structure leading to an decrease of T_2 which can be observed for most samples.

T_1 is the relaxation time where the largest changes are noticed in the experiments, but this also comes with a larger standard deviation than for T_2. The standard deviation for the reruns provided a deviation for T_1 of 6.2 % while T_2 only had a deviation of 2.5% at 20 MHz. This can be explained by how T_1 is more sensitive to experimental setups, temperature differences and uneven composition all which are present. These parameters were minimized in the experiments but not low enough to not affect the results.

T_1 could be used for the overall composition changes in milk spoilage, as large changes would imply viscosity and changes the chemical environment. However the large deviations seen in the experiments could be problematic as real changes might be hard to specify for T_1. On the other hand T_2 does not show the strongest trends over time but the low deviation, nearly always lower than errors observed at 20 MHz reruns. T_2 showed smaller changes and was more microorganisms dependent than T_1. The T_2 could be used for identifying spoilage at early stages and specifically from structural changes. The biggest outlier for T_2 measurements were in the fat region at 60 MHz, this relates back to what was earlier discussed, that it could be due to the complexity of the fat region in milk. When T_2 was observed above the standard deviation it was at later days of incubation which is not out of the ordinary. The microorganisms grow at different speeds and their mechanisms could deviate from sample to sample more at later stages, as the microbial growth is not uniform. The same trend was not seen for T_1, large deviations could be seen at different days but not consistently over instruments or microorganisms.

All microorganisms studied showed quite similar trends for relaxation times in all instruments with only a few days being outliers. For both high-field MRI and low-field NMR T_1 showed a slight increase over time, but the large standard deviation makes it a trend which cannot with certainty be identified. For T_2 an overall decrease from day 0 to day 8 were observed, with some outliers with larger deviations present.

The overall trend of all three microorganisms in this thesis showed a similar trend over incubation time. This indicates that milk spoilage for more complex systems with several microorganisms present in one sample could be detected with NMR.

4.8 Package Penetration

The possibility of using NMR through packing materials were evaluated by using different packaging materials wrapped around the same sample tube of non-contaminated milk. The relaxation times were measured for each material to understand how they would affect the signal. In 4.20 we can observe that T_1 decreases with increased complexity of material. This trend for T_1 is most likely due to how the materials interact with the RF field around the sample, directly impacting the TD-measurement. The largest decrease is for the material with the aluminium layer due to how it reacts stronger with the RF field. The observed trend correlates to how the materials disturb the accuracy leading to shorter apparent T_1 relaxation times.

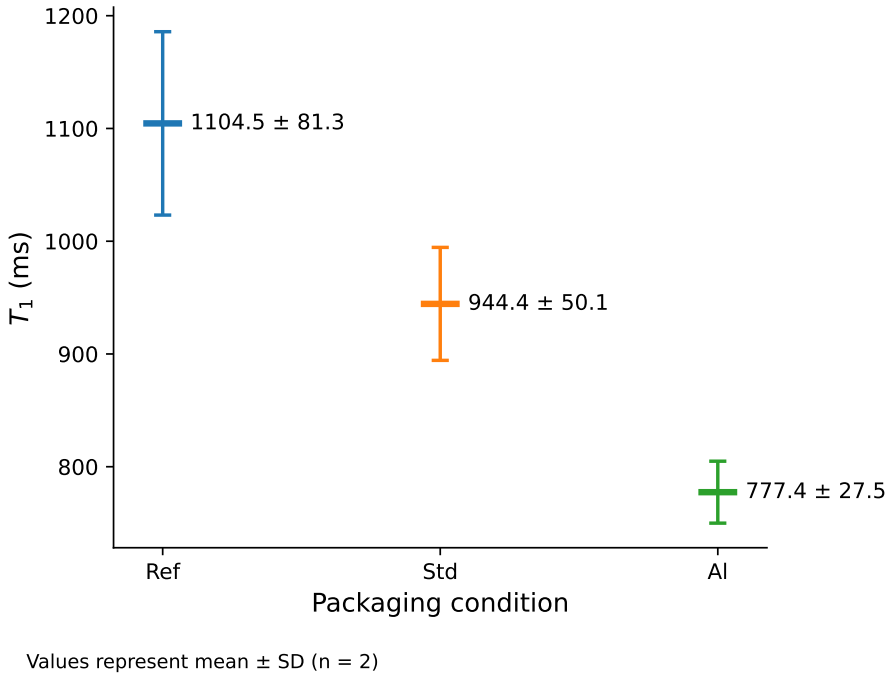

Figure 4.20: Three packaging materials (Reference, Standard packaging, Aluminium) compared with mean T_1 relaxation times (n = 2, mean ± SD)

The opposite trend was observed for T_2 where an increase between the reference sample and aluminium packaging can be observed in Figure 4.21. The raw data showed early onset of noise for aluminium packaging suggesting reduced signal quality due to RF interference, this further indicates how aluminium affects the RF Field and quality. This also influenced the fitting and caused a longer apparent T_2 rather than true relaxation change. For the standard packaging there was not as much difference observed compared to the reference, where they both lay inside of each other's SD.

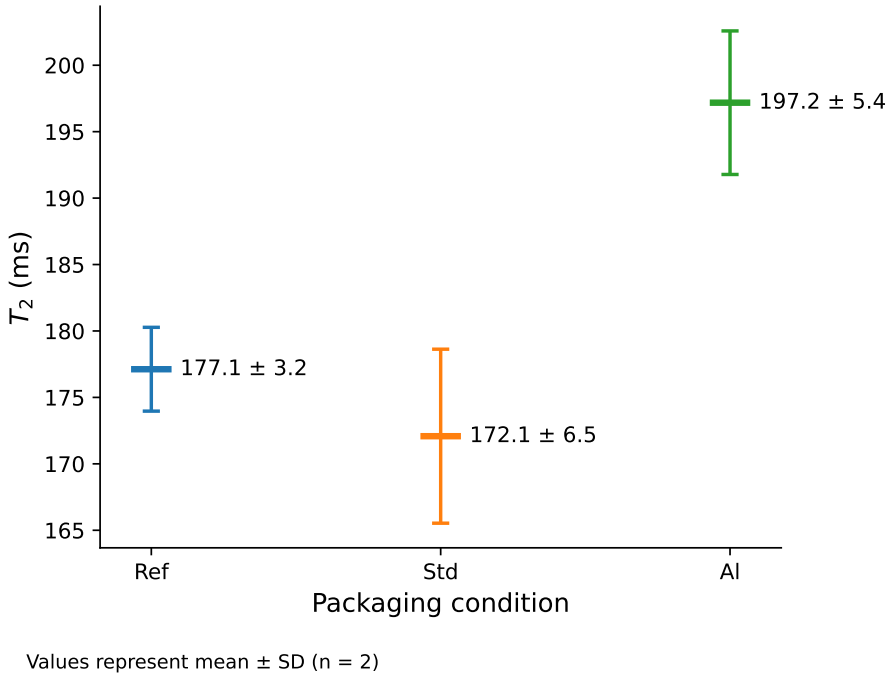

Figure 4.21: Three packaging materials (Reference, Standard packaging, Aluminium) compared with mean T_2 relaxation times (n = 2, mean ± SD)

Table 4.10: 20 MHz batch thickness values presented as mean ± SD ($n = 2$).

Packaging	T_1 **(mean ± SD)**	T_2 **(mean ± SD)**
Ref	1104.5 ± 81.3	177.1 ± 3.2
Std	944.4 ± 50.1	172.1 ± 6.5
Al	777.4 ± 27.5	197.2 ± 5.4

These observations indicate that packaging thickness influences the apparent relaxation instead of true values. The changes seen are therefore not from differences in the sample but instead from conductive shielding and the experimental setup. From Table 4.10 we can see that it is possible to detect both T_1 and T_2 with the two different packaging materials investigated, the raw data points are presented in Appendix B. This indicates that it is possible to use 20 MHz TD-NMR for measurements on relaxation times in an in-line process. This provides a good understanding for how relaxation times get affected from packing material and especially the interference seen from the aluminium layer.

4.9 Implementations for an In-Line Spoilage Detection Process

For further investigations into milk spoilage with NMR, T_2 would be of most interest. Less impact from uncertainty in the experimental setups and lower standard deviation ensures large changes measured comes from spoilage and not instrument error.

The Bruker minispec 20 MHz were able to show trends over incubation time. It also showed that measurements could be performed through packaging materials at a low magnetic field strength. An in-line process with a low-field TD-NMR could be possible with more fine tuning of the experimental setup and fitting functions for relaxation time extraction.

4.10 Recommendations for Further Research

Future studies should work on extending the understanding of how contaminations in milk affect the relaxation times. This thesis provided the understanding that it is possible to see the differences and future work should focus on the usage of a single instrument. Investigating how a TD-NMR would work in an in-line process by optimizing the experimental setup and fitting models for extracting relaxation times. This could be done by using more replicates for better understanding of replicability and if the trends still are present. The same sample should be used over time to get an understanding of what really happens in a specific sample from microbial growth. The studied sample could also contain different microorganisms to study how they interact together. It should also be discussed how shaking the sample before testing would affect the results as this would remove any separation of layers that may occur during incubation.

5
Conclusion

Through extensive research this thesis provided indications that milk spoilage can be detected using NMR. It further showed how different magnetic field strengths provided similar trends. There is potential to use a low-field NMR for future industry implementations but more work is needed to confirm this potential. Further the thesis provided information about how measured relaxation times could deviate in a single sample from heterogeneity, but also from instrument errors.

The thesis demonstrated how a low field TD-NMR at 20 MHz would be able to detect spoilage through packaging materials. However the values obtained were apparent relaxation times and not true values which could hinder the interpretation of the data.

Early on it could be seen that diffusion would not be able to be used for an in-line process as it was slow and the data was not useful for this purpose. The research showed that T_2 provided the lowest standard deviation, however the trends were not strong and large sample to sample variation was observed. T_1 showed higher standard deviation with a slight increase over time. From T_1 in the water dominated region the most clear trend could be observed, indicating how the chemical environment is changing due to contamination. No clear choice could be seen with respect to relaxation times, but it demonstrated that NMR signal is affected by milk spoilage, and more research needs to be done to build on the findings.

The complexity of milk spoilage was shown and how several different microorganisms in the same sample makes the choices for an in-line process diverse. The thesis demonstrated how relaxation times for all microorganisms showed a similar trend over time. This could be seen even though the metabolic activity of them varied, this indicates that milk spoilage affects relaxation times in similar manners between the microorganisms studied.

Finally, low-field NMR shows potential to be a useful instrument for detection of milk spoilage in industry, although more research needs to be done to understand the reliability of the measured MR observed, to clarify their relationship with spoilage mechanisms, and to fine tune the measurement methodology. This thesis has provided a broader understanding about how milk spoilage affects relaxation times and suggests that low-field NMR could be a viable method for spoilage detection.

5.1 Disclosure and Declaration of AI Use

AI assistance was used to a limited extent during the preparation of this work. Assistance was occasionally used for programming and data processing, as well as for reviewing grammar and spelling.

Bibliography

[1] Hanna Górska-Warsewicz et al. "Milk and Dairy Products and Their Nutritional Contribution to the Average Polish Diet". In: *Nutrients* 11.8 (Aug. 2019), p. 1771. ISSN: 2072-6643. DOI: 10.3390/nu11081771.

[2] Dilip Kumar et al. "Compositional Quality of Milk and Its Contaminants on Physical and Chemical Concern: A Review". In: *International Journal of Current Microbiology and Applied Sciences* 7 (May 2018), pp. 1125–1132. DOI: 10.20546/ijcmas.2018.705.137.

[3] Antonio Bevilacqua, Maria Rosaria Corbo, and Milena Sinigaglia. *The microbiological quality of food: foodborne spoilers*. eng. Woodhead Publishing series in food science, technology and nutrition. Woodhead Publishing Elsevier, 2017. Chap. 7, pp. 151–178. ISBN: 978-0-08-100502-6.

[4] Tetra. *UHT Milk FAQ*. en. URL: https://www.tetrapak.com/insights/food-categories/dairy/uht-faq.

[5] "Recent advances in time domain NMR & MRI sensors and their food applications". en-US. In: *Current Opinion in Food Science* 17 (Oct. 2017), pp. 9–15. ISSN: 2214-7993. DOI: 10.1016/j.cofs.2017.07.005.

[6] Christel Cederberg and Ulf Sonesson. *Global food losses and food waste: extent, causes and prevention; study conducted for the International Congress Save Food! at Interpack 2011, [16 - 17 May], Düsseldorf, Germany*. en. Ed. by Jenny Gustavsson. Meeting Name: International Congress Save Food! Rome: Food and Agriculture Organization of the United Nations, 2011. ISBN: 978-92-5-107205-9.

[7] Karen Fisher and Dan Whittaker. "WRAP's vision is a world in which resources are used sustainably." en. In: ().

[8] *Milk composition*. en. URL: https://www.fao.org/dairy-production-products/products/milk-composition/en.

[9] *The basic workings of milk homogenization*. en. URL: https://www.tetrapak.com/insights/cases-articles/basic-workings-of-milk-homogenization.

[10] Seyed Hossein Davoodi et al. "Health-Related Aspects of Milk Proteins". In: *Iranian Journal of Pharmaceutical Research : IJPR* 15.3 (2016), pp. 573–591. ISSN: 1735-0328. URL: https://pmc.ncbi.nlm.nih.gov/articles/PMC5149046/.

[11] Aili Li et al. "Advances in Low-Lactose/Lactose-Free Dairy Products and Their Production". In: *Foods* 12.13 (June 2023), p. 2553. ISSN: 2304-8158. DOI: 10.3390/foods12132553.

[12] Enrique Romero-Velarde et al. “The Importance of Lactose in the Human Diet: Outcomes of a Mexican Consensus Meeting”. In: *Nutrients* 11.11 (Nov. 2019), p. 2737. ISSN: 2072-6643. DOI: 10.3390/nu11112737.

[13] Lisa Quigley et al. “The complex microbiota of raw milk”. In: *FEMS Microbiology Reviews* 37.5 (Sept. 2013), pp. 664–698. ISSN: 0168-6445. DOI: 10.1111/1574-6976.12030.

[14] *RAW MILK QUALITY | Dairy Processing Handbook*. en. URL: http://dairyprocessinghandbook.tetrapak.com/chapter/raw-milk-quality.

[15] *UHT Dairy Products Market Growth, Long-Shelf-Life Dairy & Market Trends*. en. URL: https://www.futuremarketinsights.com/reports/uht-dairy-products-market.

[16] Erin R. Sanders. “Aseptic Laboratory Techniques: Plating Methods”. en. In: *Journal of Visualized Experiments (JoVE)* 63 (May 2012), e3064. ISSN: 1940-087X. DOI: 10.3791/3064.

[17] Mohamed Ziyaina, Barbara Rasco, and Shyam S. Sablani. “Rapid methods of microbial detection in dairy products”. en. In: *Food Control* 110 (Apr. 2020), p. 107008. ISSN: 09567135. DOI: 10.1016/j.foodcont.2019.107008.

[18] Katherine M. McKinnon. “Flow Cytometry: An Overview”. In: *Current protocols in immunology* 120 (Feb. 2018), pp. 5.1.1–5.1.11. ISSN: 1934-3671. DOI: 10.1002/cpim.40.

[19] Ronald Ross Watson and Victor R. Preedy. *Dietary interventions in gastrointestinal diseases: foods, nutrients, and dietary supplements*. Academic press, 2019. Chap. 22, pp. 265–275. ISBN: 978-0-12-814469-5.

[20] Cian D. Hickey et al. “Growth and location of bacterial colonies within dairy foods using microscopy techniques: a review”. In: *Frontiers in Microbiology* 6 (Feb. 2015), p. 99. ISSN: 1664-302X. DOI: 10.3389/fmicb.2015.00099.

[21] *Psychrotrophic*. en-US. Section: Vol 13 Issue 2. June 2019. URL: https://microbiologyjournal.org/psychrotrophic-microbiota-in-milk-and-fermented-milk-products/.

[22] “Application of NMR spectroscopy to milk and dairy products”. en-US. In: *Trends in Food Science & Technology* 10.10 (Oct. 1999), pp. 313–320. ISSN: 0924-2244. DOI: 10.1016/S0924-2244(00)00012-1.

[23] Andrew R. Barron. “Physical Methods In Chemistry And Nano Science”. In: Midas Green Innovations, Ltd, 2012. Chap. 3.7, pp. 321–255.

[24] Patrick Giraudeau, Virginie Silvestre, and Serge Akoka. “Optimizing water suppression for quantitative NMR-based metabolomics: a tutorial review”. en. In: *Metabolomics* 11.5 (Oct. 2015), pp. 1041–1055. ISSN: 1573-3890. DOI: 10.1007/s11306-015-0794-7.

[25] *Shimming - an overview | ScienceDirect Topics*. URL: https://www.sciencedirect.com/topics/medicine-and-dentistry/shimming.

[26] James Keeler. *Understanding NMR Spectroscopy*. 2nd ed. John Wiley Sons Inc, 2010. ISBN: 9780470746097.

[27] Perry Sprawls. *Magnetic Resonance Imaging: Principles, Methods, and Techniques*. Medical Physics Publishing, 2000. ISBN: 9780944838976.

[28] François Mariette. “NMR Relaxometry and Imaging of Dairy Products”. en. In: *Modern Magnetic Resonance*. Springer, Cham, 2017, pp. 1–23. ISBN: 978-3-319-28275-6. DOI: 10.1007/978-3-319-28275-6_38-1.

[29] Hans Koss, Mark Rance, and Arthur G. Palmer. “General Expressions for Carr—Purcell—Meiboom—Gill Relaxation Dispersion for N-Site Chemical Exchange”. In: *Biochemistry* 57.31 (Aug. 2018), pp. 4753–4763. ISSN: 0006-2960. DOI: 10.1021/acs.biochem.8b00370.

[30] Franz Dalitz et al. “Process and reaction monitoring by low-field NMR spectroscopy”. In: *Progress in Nuclear Magnetic Resonance Spectroscopy* 60 (Jan. 2012), pp. 52–70. ISSN: 0079-6565. DOI: 10.1016/j.pnmrs.2011.11.003.

[31] Hamed Ebrahimnejad et al. “Use of Magnetic Resonance Imaging in Food Quality Control: A Review”. In: *Journal of Biomedical Physics & Engineering* 8.1 (Mar. 2018), pp. 127–132. ISSN: 2251-7200. URL: https://pmc.ncbi.nlm.nih.gov/articles/PMC5928302/.

[32] David Milford et al. “Mono-Exponential Fitting in T2-Relaxometry: Relevance of Offset and First Echo”. In: *PLoS ONE* 10.12 (Dec. 2015), e0145255. ISSN: 1932-6203. DOI: 10.1371/journal.pone.0145255.

[33] Ronald K. June, John P. Cunningham, and David P. Fyhrie. “A Novel Method for Curvefitting the Stretched Exponential Function to Experimental Data”. In: *Biomedical engineering research* 2.4 (Dec. 2013), pp. 153–158. ISSN: 2306-6008. DOI: 10.5963/ber0204001.

[34] C. Da Silva et al. “Gamma distribution function to understand anaerobic digestion kinetics: Kinetic constants are not constant”. In: *Chemosphere* 306 (Nov. 2022), p. 135579. ISSN: 0045-6535. DOI: 10.1016/j.chemosphere.2022.135579.

[35] Scott I. Vrieze. “Model selection and psychological theory: A discussion of the differences between the Akaike Information Criterion (AIC) and the Bayesian Information Criterion (BIC)”. In: *Psychological Methods* 17.2 (June 2012), pp. 228–243. ISSN: 1082-989X. DOI: 10.1037/a0027127.

[36] Magritek. *Determination of Fat, Lactose and Water Content in Milk*. https://magritek.com/wp-content/uploads/2021/02/Determination-of-fat-lactose-and-water-content-in-milk.pdf. Application note, Spinsolve benchtop NMR spectrometer. n.d.

A

Repeated Measurements

Nr	T_1 **(ms)**	T_2 **(ms)**
1	1247.77	177.98
2	1307.03	177.95
3	1145.17	185.58
4	1144.00	175.93
5	1157.00	184.69

Table A.1: Raw repeated measurements at 20 MHz used for calculation of mean and standard deviation.

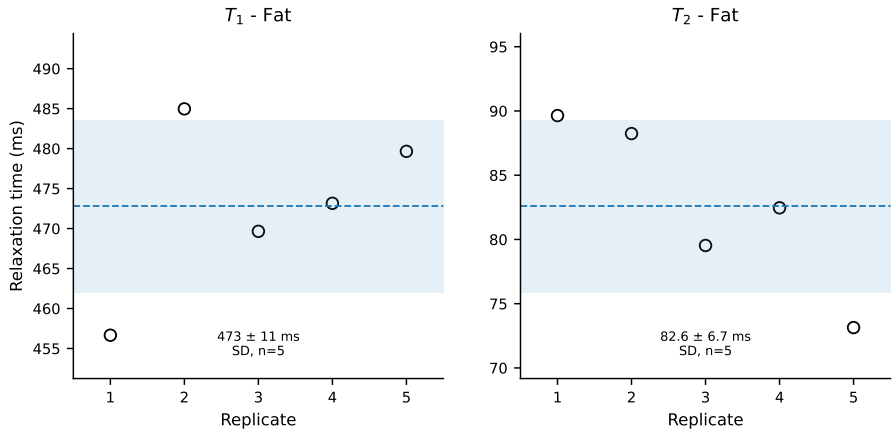

Figure A.1: Five repeated T_1 and T_2 measurements at 60 MHz for the fat region.

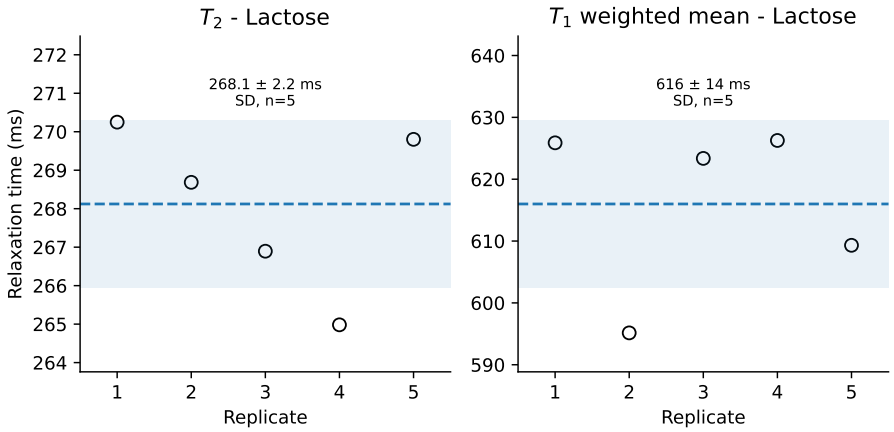

Figure A.2: Five repeated T_1 and T_2 measurements at 60 MHz for the lactose region

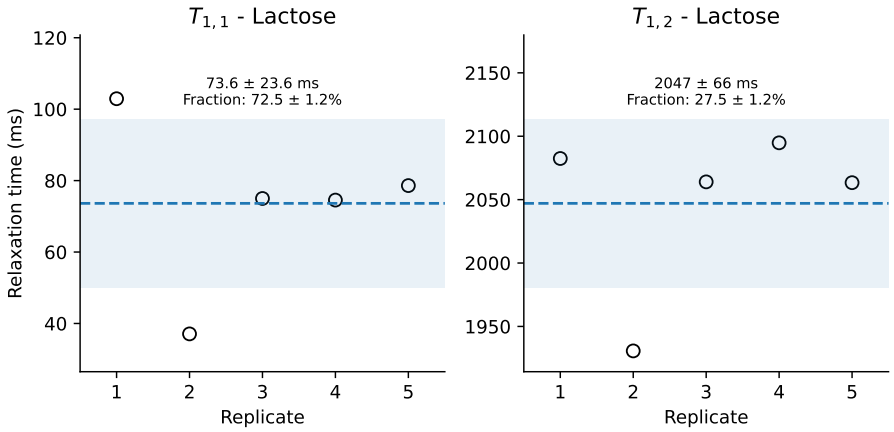

Figure A.3: Five repeated $T_{1,1}$ and $T_{1,2}$ measurements at 60 MHz for the lactose region

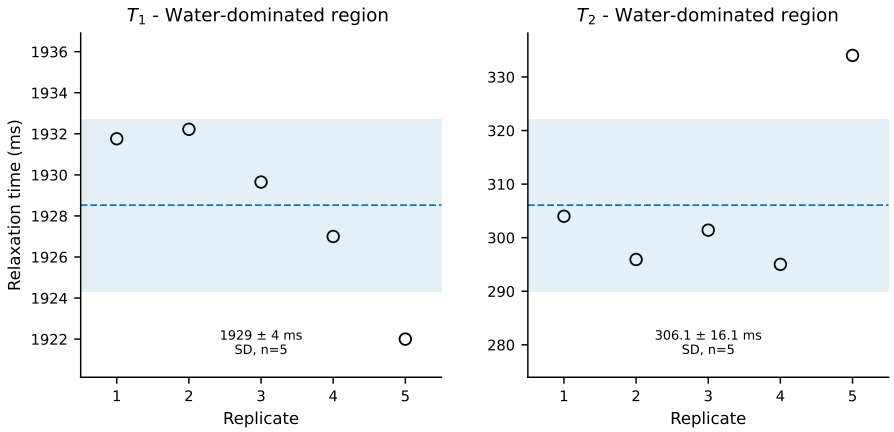

Figure A.4: Five repeated T_1 and T_2 measurements at 60 MHz for the water dominated region region

B

Data from Thickness Measurements

Packaging	T_1 **(ms)**	T_2 **(ms)**
Ref	1162	174.89
Ref	1047	179.35
Std	979.85	167.45
Std	909	176.71
Al	758	201.00
Al	796.85	193.36

Table B.1: Raw data at 20 MHz for thickness measurements used for calculation of mean and standard deviation.

C

Bruker Minispec Mq 20 MHz Data and Plots

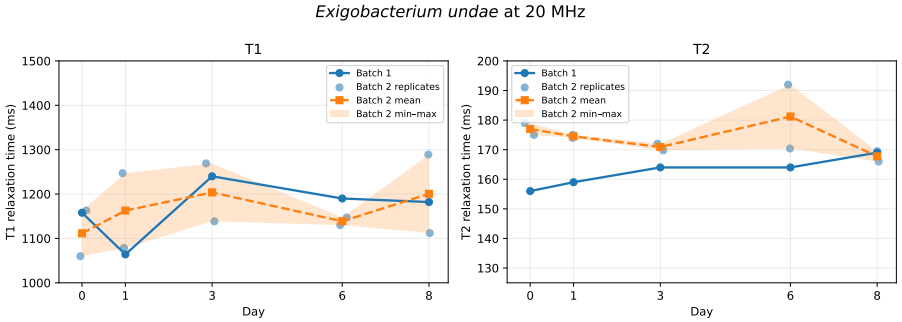

Figure C.1: Raw relaxation time data for *Exiguobacterium undae* visualized for batch 1 and batch 2 with replicates, measured at 20 MHz . Shaded region representing the standard deviation from batch 2.

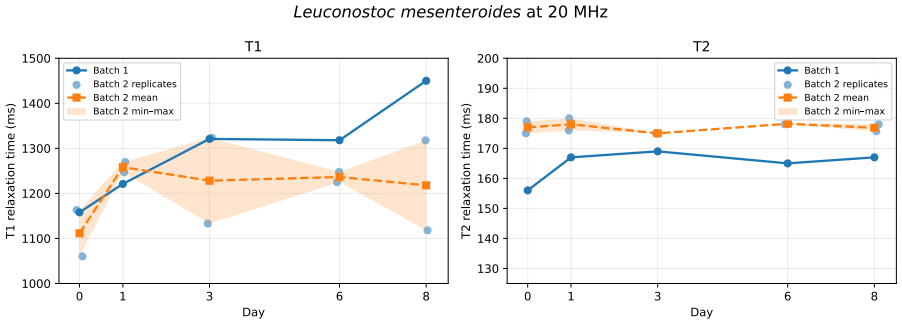

Figure C.2: Raw relaxation time data for *Leuconostoc mesenteroides* visualized for batch 1 and batch 2 with replicates, measured at 20 MHz . Shaded region representing the standard deviation from batch 2.

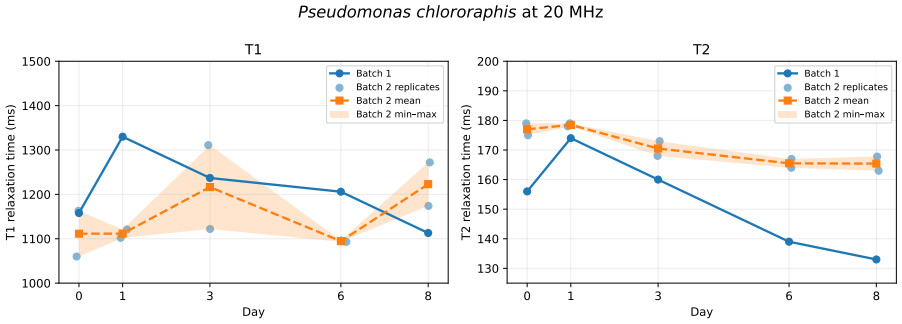

Figure C.3: Raw relaxation time data for *Pseudomonas chlororaphis* visualized for batch 1 and batch 2 with replicates, measured at 20 MHz. Shaded region representing the standard deviation from batch 2.

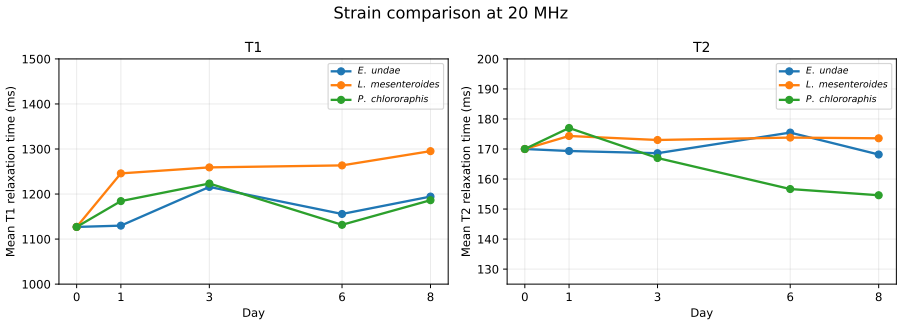

Figure C.4: Mean T_1 and T_2 relaxation times for *E. undae, L. mesenteroides*, and *P. chlororaphis* for batch 2 and batch 1 combined, measured at 20 MHz

Table C.1: Raw data of T_1 and T_2 relaxation time dataset at 20 MHz for Batch 1 and Batch 2 with replicates.

Batch	Replicate	Strain	Day	T1 (ms)	T2 (ms)
1	–	E	0	1158	156
1	–	E	1	1064	159
1	–	E	3	1240	164
1	–	E	6	1190	164
1	–	E	8	1182	169
1	–	L	0	1158	156
1	–	L	1	1221	167
1	–	L	3	1321	169
1	–	L	6	1318	165
1	–	L	8	1450	167
1	–	P	0	1158	156
1	–	P	1	1330	174
1	–	P	3	1237	160
1	–	P	6	1206	139
1	–	P	8	1113	133
2	R1	E	0	1162.90	175.0
2	R1	E	1	1078.55	175.0
2	R1	E	3	1138.45	169.8
2	R1	E	6	1147.25	170.4
2	R1	E	8	1112.12	169.5
2	R1	L	0	1162.90	175.0
2	R1	L	1	1269.58	180.0
2	R1	L	3	1323.47	175.0
2	R1	L	6	1247.77	178.0
2	R1	L	8	1317.70	178.0
2	R1	P	0	1162.90	175.0
2	R1	P	1	1102.00	178.0
2	R1	P	3	1122.00	168.0
2	R1	P	6	1096.00	164.0
2	R1	P	8	1174.00	167.8
2	R2	E	0	1060	179.0
2	R2	E	1	1247	174.0
2	R2	E	3	1269	172.0
2	R2	E	6	1130	192.0
2	R2	E	8	1289	166.0
2	R2	L	0	1060	179.0
2	R2	L	1	1247	176.0
2	R2	L	3	1133	175.0
2	R2	L	6	1225	178.4
2	R2	L	8	1118	175.7
2	R2	P	0	1060	179.0
2	R2	P	1	1121	179.0
2	R2	P	3	1311	173.0
2	R2	P	6	1093	167.0
2	R2	P	8	1272	163.0

D

Magritek Spinsolve 60 MHz Data and Plots

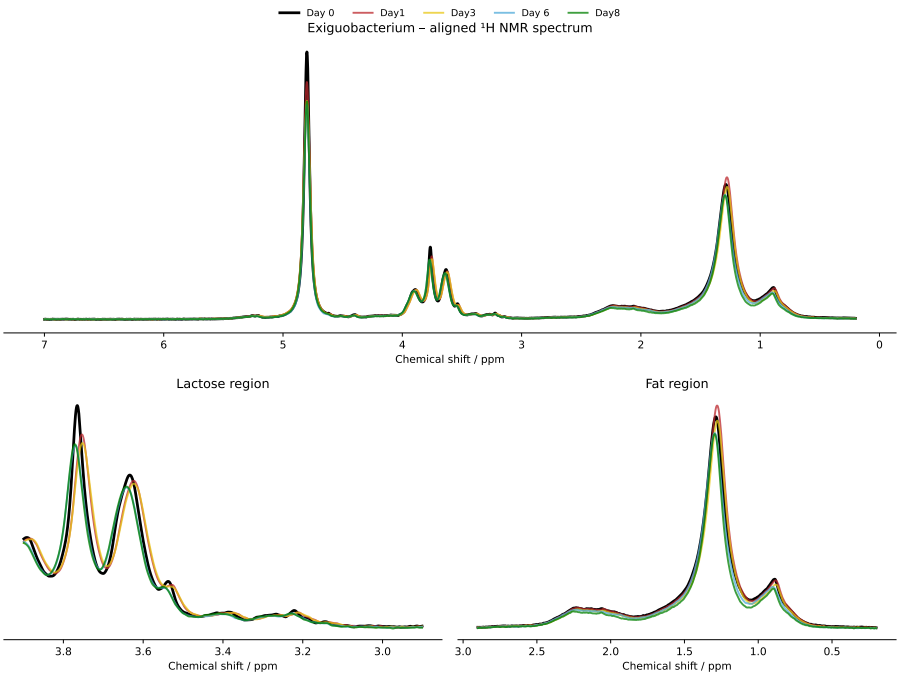

Figure D.1: Aligned ^{1}H NMR spectra for replicate 1 in batch 2 of *E. undae*, highlighting changes in the lactose and fat regions

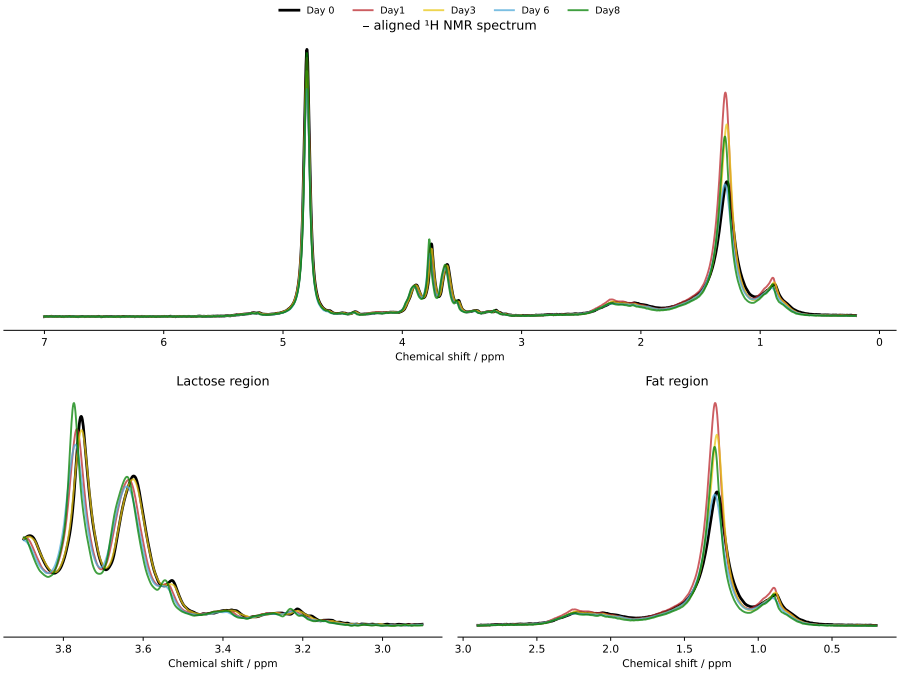

Figure D.2: Aligned ^{1}H NMR spectra for replicate 2 in batch 2 of *E. undae*, highlighting changes in the lactose and fat regions

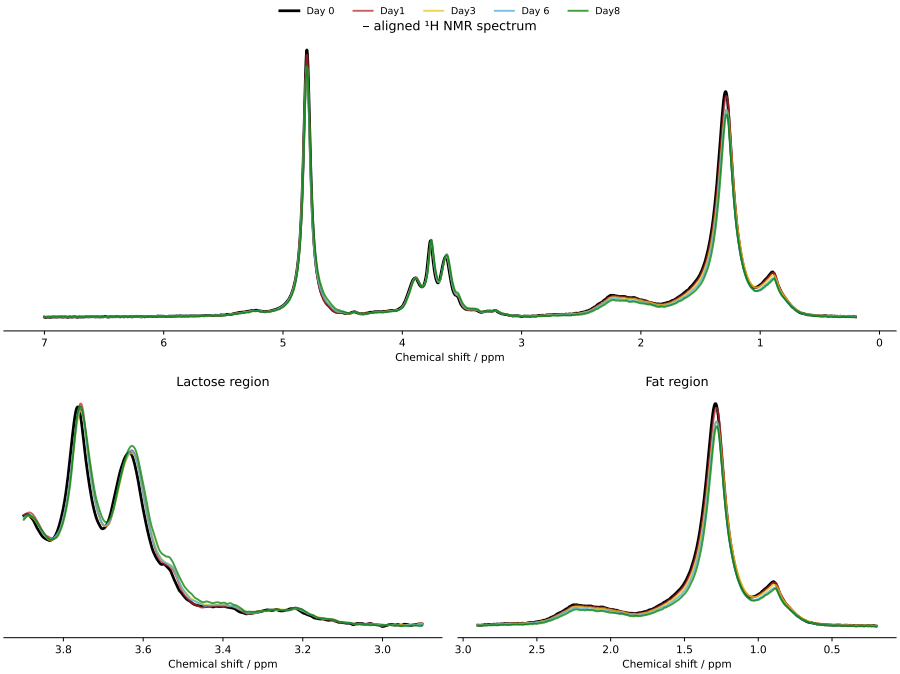

Figure D.3: Aligned ^{1}H NMR spectra for batch 1 of *L. mesenteroides*, highlighting changes in the lactose and fat regions

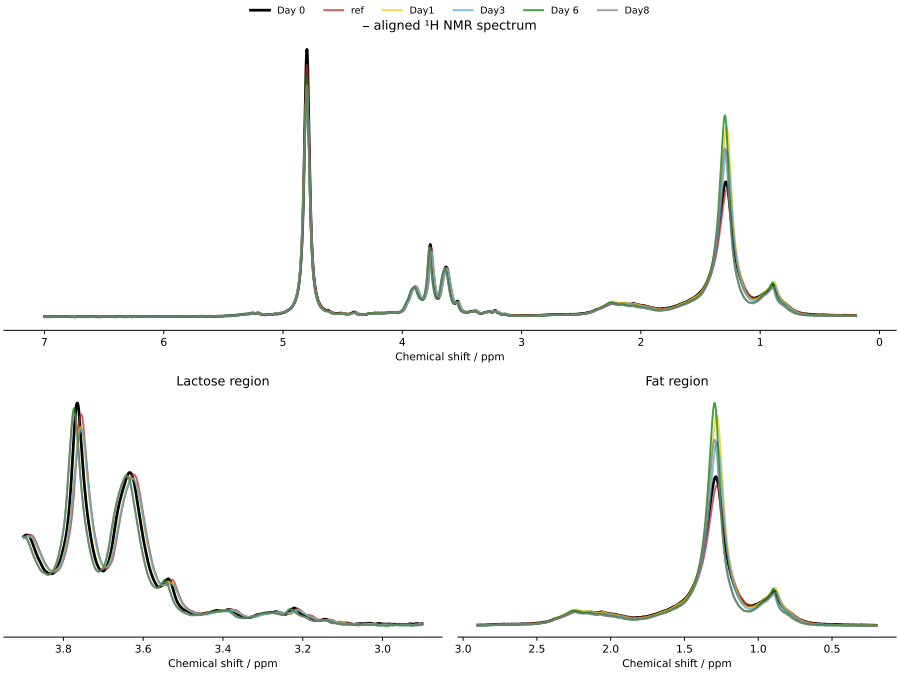

Figure D.4: Aligned ^{1}H NMR spectra for replicate 2 in batch 2 of *L. mesenteroides*, highlighting changes in the lactose and fat regions

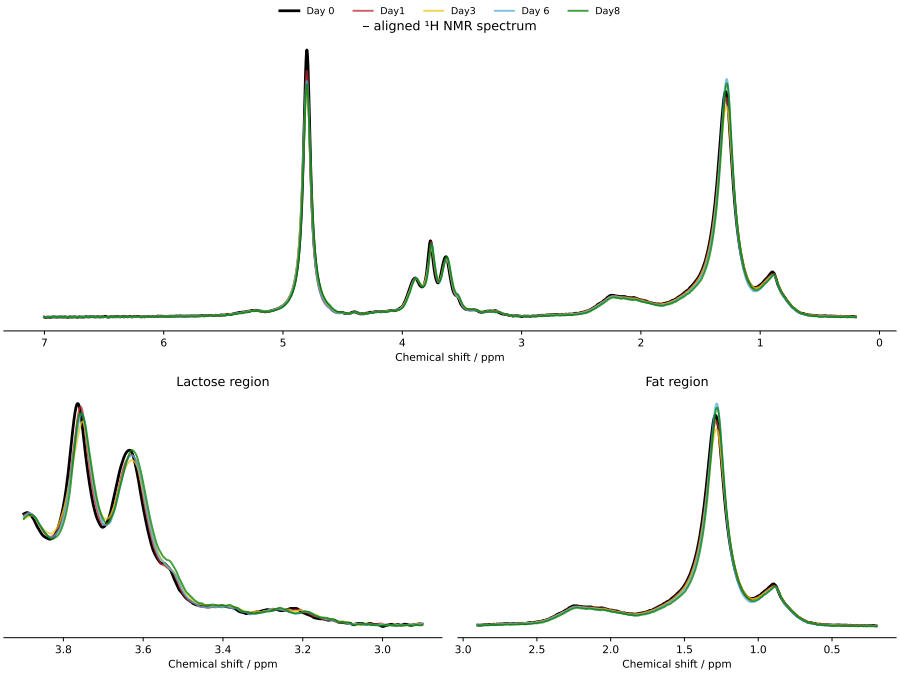

Figure D.5: Aligned ^{1}H NMR spectra for batch 1 of *P. chlororaphis*, highlighting changes in the lactose and fat regions

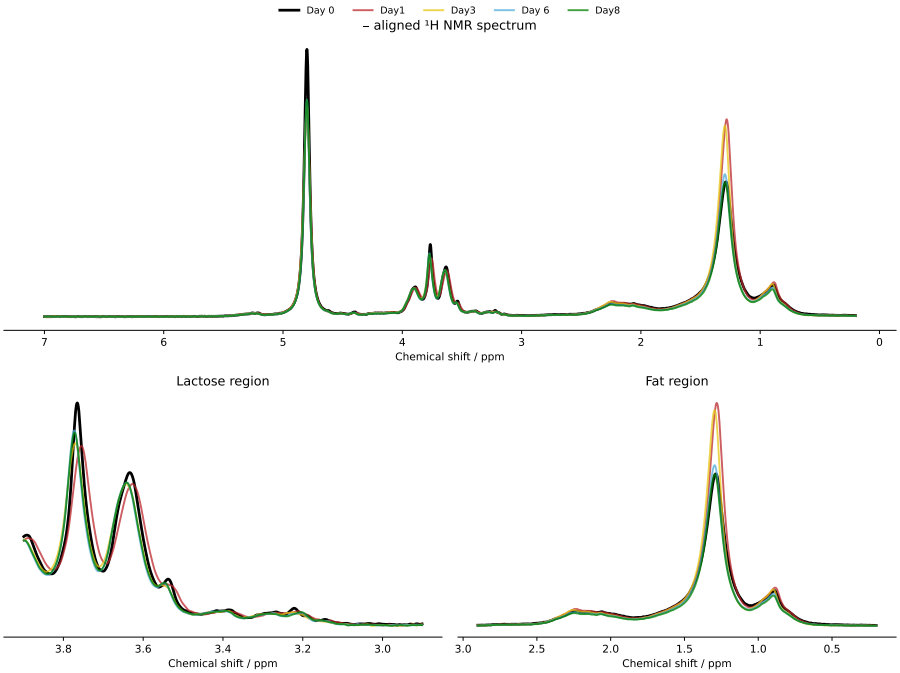

Figure D.6: Aligned ^{1}H NMR spectra for replicate 2 in batch 2 of *P. chlororaphis*, highlighting changes in the lactose and fat regions

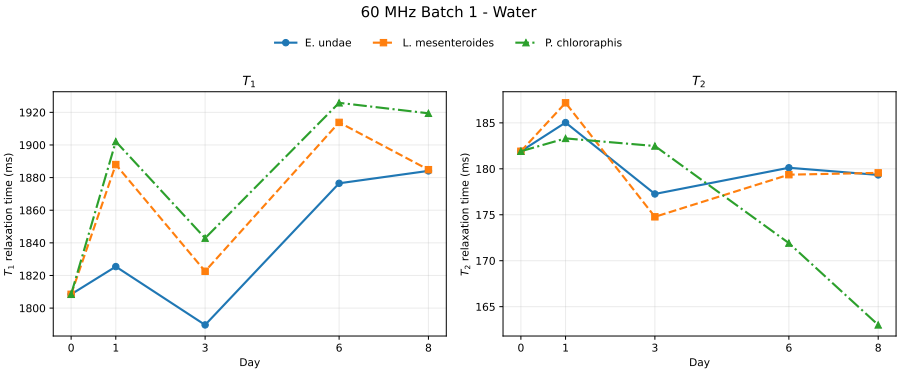

Figure D.7: $T_{1,1}$, $T_{1,2}$,weighted T_1 and T_2 relaxation times for *E. undae, L. mesenteroides*, and *P. chlororaphis* for batch 1 measured at 60 MHz for the water dominated region.

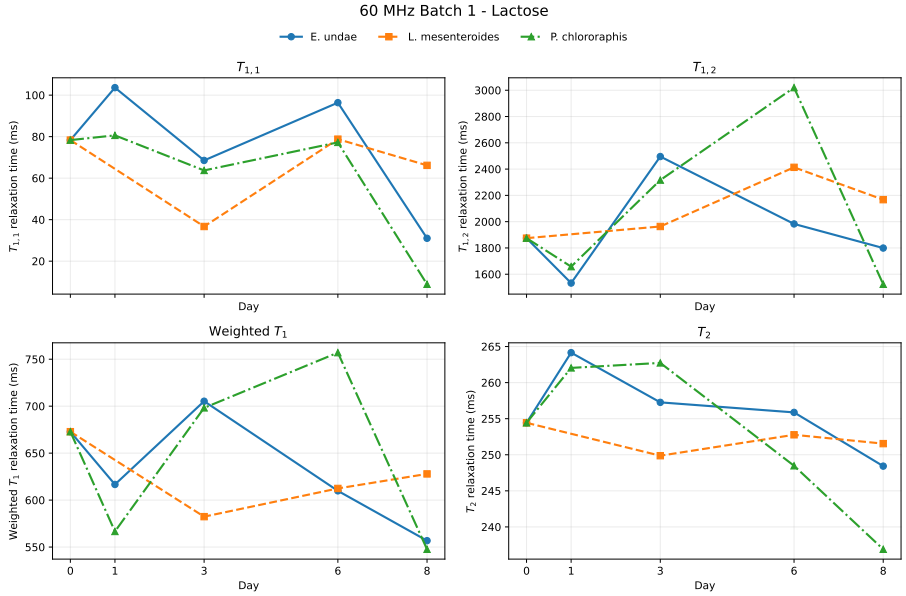

Figure D.8: $T_{1,1}$, $T_{1,2}$,weighted T_1 and T_2 relaxation times for *E. undae, L. mesenteroides*, and *P. chlororaphis* for batch 1 measured at 60 MHz for the lactose region.

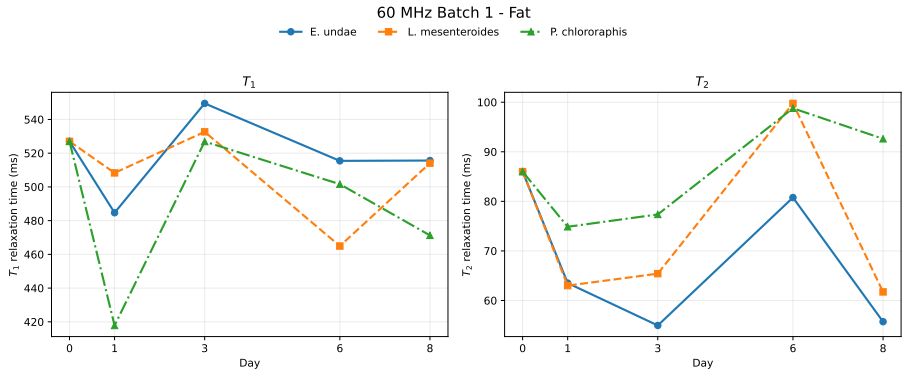

Figure D.9: $T_{1,1}$, $T_{1,2}$,weighted T_1 and T_2 relaxation times for *E. undae, L. mesenteroides*, and *P. chlororaphis* for batch 1 measured at 60 MHz for the fat region.

Table D.1: Relaxation times for the water region measured at 60 MHz.

Water			
Batch 1			
Strain	Day	T_1	T_2
E	0	1808.45	181.91
E	1	1825.45	185.03
E	3	1789.59	177.26
E	6	1876.61	180.11
E	8	1884.12	179.34
L	0	1808.45	181.91
L	1	1887.98	187.19
L	3	1822.58	174.78
L	6	1913.84	179.36
L	8	1884.85	179.56
P	0	1808.45	181.91
P	1	1902.12	183.31
P	3	1842.88	182.48
P	6	1925.83	171.92
P	8	1919.42	163.01
Batch 2 Replicate 1			
E	0	1743.54	323.20
E	1	1725.01	334.33
E	3	1807.65	317.23
E	6	1955.60	330.63
E	8	1870.16	315.71
L	0	1743.54	323.20
L	1	1783.66	321.33
L	3	1784.85	318.03
L	6	1912.13	344.83
L	8	1950.18	312.02
P	0	1743.54	323.20
P	1	1874.88	333.34
P	3	1807.79	317.56
P	6	1932.05	347.92
P	8	1937.88	335.67
Batch 2 Replicate 2			
E	0	1674.39	321.89
E	1	1760.56	343.93
E	3	1847.76	305.73
E	6	1867.70	323.77
E	8	1872.97	348.15
L	0	1674.39	321.89
L	1	1784.59	316.92
L	3	1868.42	329.67
L	6	1931.76	304.00
L	8	1957.54	332.25
P	0	1674.39	321.89
P	1	1877.20	346.18
P	3	1909.49	311.67
P	6	1930.60	323.49
P	8	1943.48	296.60

Table D.2: Relaxation times for the fat region measured at 60 MHz.

Fat			
Batch 1			
Strain	Day	T_1	T_2
E	0	527.00	86.00
E	1	484.68	63.51
E	3	549.51	54.96
E	6	515.44	80.77
E	8	515.64	55.72
L	0	527.00	86.00
L	1	508.30	63.00
L	3	532.66	65.41
L	6	464.94	99.76
L	8	514.10	61.73
P	0	527.00	86.00
P	1	417.84	74.87
P	3	526.89	77.36
P	6	501.62	98.78
P	8	471.27	92.62
Batch 2 Replicate 1			
E	0	456.24	47.18
E	1	462.71	43.76
E	3	463.87	52.09
E	6	559.51	41.24
E	8	508.45	34.03
L	0	456.24	47.18
L	1	569.85	55.14
L	3	598.62	45.95
L	6	462.53	36.25
L	8	505.07	39.76
P	0	456.24	47.18
P	1	463.20	45.91
P	3	570.00	47.80
P	6	459.52	36.16
P	8	487.79	38.20
Batch 2 Replicate 2			
E	0	570.98	34.30
E	1	426.20	69.95
E	3	460.42	78.54
E	6	470.07	54.39
E	8	440.92	72.90
L	0	570.98	34.30
L	1	567.65	64.23
L	3	461.46	70.45
L	6	456.66	89.64
L	8	475.59	59.10
P	0	570.98	34.30
P	1	440.49	73.12
P	3	447.23	68.38
P	6	506.01	71.47
P	8	479.62	68.10

Table D.3: Relaxation times for the lactose region measured at 60 MHz.

Lactose							
Batch 1							
Strain	Day	$T_{1,1}$	$F_{T_{1,1}}$	$T_{1,2}$	$F_{T_{1,2}}$	Weighted T_1	T_2
E	0	78.34	66.90	1874.43	33.10	672.85	254.43
E	1	103.62	64.10	1532.71	35.90	616.64	264.15
E	3	68.54	73.77	2495.60	26.24	705.28	257.26
E	6	96.38	72.78	1982.73	27.22	609.85	255.87
E	8	31.03	70.26	1799.18	29.74	556.80	248.42
L	0	78.34	66.90	1874.43	33.10	672.85	254.43
L	1	567.57	86.12	4319.90	13.88	1088.24	260.94
L	3	36.07	71.16	1963.31	28.84	590.37	249.87
L	6	78.79	77.14	2413.42	22.86	612.41	252.77
L	8	66.11	73.27	2167.37	26.73	627.88	251.54
P	0	78.34	66.90	1874.43	33.10	672.85	254.43
P	1	80.62	69.18	1657.76	30.82	566.62	262.04
P	3	63.73	71.92	2316.37	28.07	696.20	262.73
P	6	77.23	76.81	3019.84	23.19	756.93	248.47
P	8	8.87	64.43	1523.63	35.57	547.64	236.90
Batch 2 Replicate 1							
E	0	67.59	67.00	1421.55	33.00	514.40	268.73
E	1	100.36	63.85	1302.40	36.16	534.39	268.36
E	3	81.68	68.78	1659.30	31.22	574.18	263.40
E	6	80.85	77.18	2430.01	22.82	617.04	268.75
E	8	74.34	71.67	1821.83	28.33	569.40	262.75
L	0	67.59	67.00	1421.55	33.00	514.40	268.73
L	1	78.19	70.78	1915.29	29.22	615.04	268.26
L	3	73.02	70.70	2172.19	29.30	688.08	270.06
L	6	9.39	72.82	1682.03	27.18	464.06	264.76
L	8	78.97	69.02	1693.53	30.98	579.23	270.59
P	0	67.59	67.00	1421.55	33.00	514.40	268.73
P	1	67.62	69.25	1598.65	30.75	538.33	271.92
P	3	16.01	75.79	2323.45	24.21	574.55	272.21
P	6	56.16	70.22	1784.26	29.78	570.71	269.21
P	8	83.81	69.16	1772.73	30.84	604.69	262.13
Batch 2 Replicate 2							
E	0	75.76	70.50	1883.00	29.60	610.78	272.86
E	1	44.19	71.55	1670.85	28.45	506.95	266.11
E	3	77.05	71.44	1842.22	28.56	581.12	269.88
E	6	75.43	70.02	1809.34	29.97	595.12	265.05
E	8	64.61	69.86	1747.04	30.14	571.62	272.21
L	0	75.76	70.50	1883.00	29.60	610.78	272.86
L	1	72.71	71.92	2362.34	28.08	715.64	269.22
L	3	82.08	72.30	1724.77	27.70	537.14	268.49
L	6	102.92	73.58	2082.44	26.42	625.83	270.25
L	8	77.30	70.21	1736.76	29.79	571.68	269.07
P	0	75.76	70.50	1883.00	29.60	610.78	272.86
P	1	37.84	71.45	1808.79	28.55	543.42	273.92
P	3	76.42	70.91	1800.20	29.09	577.88	262.65
P	6	44.70	69.61	2098.81	30.39	668.89	260.18
P	8	84.66	69.42	1852.18	30.58	625.16	261.85

E

Bruker Avance 300 MHz MRI Data and Plots

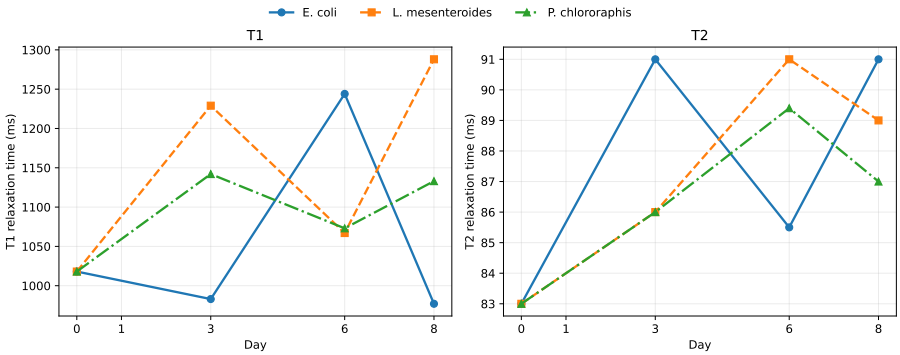

Figure E.1: T_1 and T_2 relaxation times for *E. undae*, *L. mesenteroides*, and *P. chlororaphis* for batch, measured at 20 MHz

Strain	Day	T_1 (ms)	T_2 (ms)
E	0	1158	156
E	1	1064	159
E	3	1240	164
E	6	1190	164
E	8	1182	169
L	0	1158	156
L	1	1221	167
L	3	1321	169
L	6	1318	165
L	8	1450	167
P	0	1158	156
P	1	1330	174
P	3	1237	160
P	6	1206	139
P	8	1113	133

Table E.1: Raw relaxation times data for batch 1 at 300 MHz.

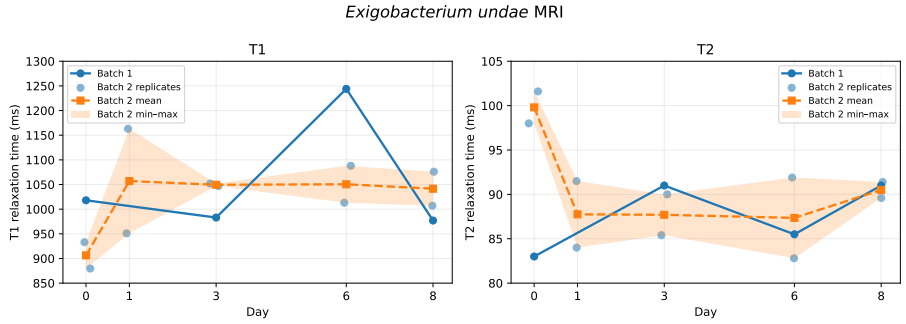

Figure E.2: Raw relaxation time data for *Exiguobacterium undae* visualized for batch 1 and batch 2 with replicates, measured at 20 MHz. Shaded region representing the standard deviation from batch 2.

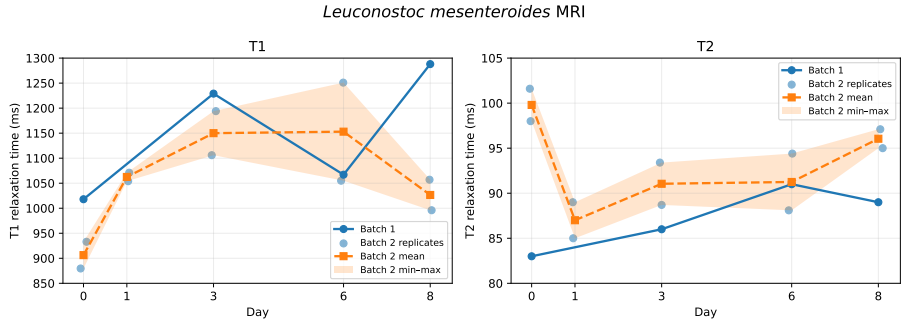

Figure E.3: Raw relaxation time data for *Leuconostoc mesenteroides* visualized for batch 1 and batch 2 with replicates, measured at 20 MHz. Shaded region representing the standard deviation from batch 2.

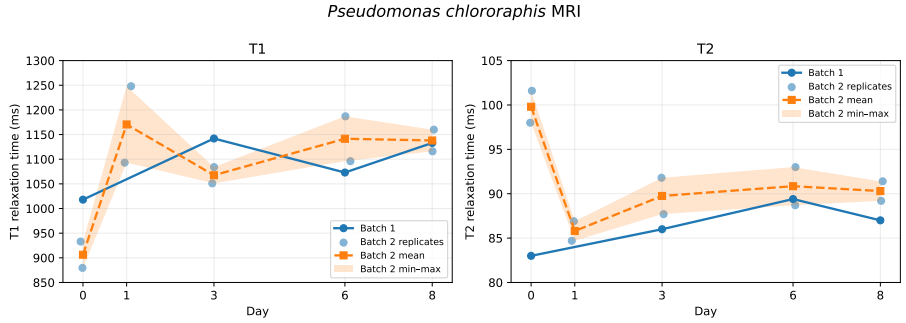

Figure E.4: Raw relaxation time data for *Pseudomonas chlororaphis* visualized for batch 1 and batch 2 with replicates, measured at 20 MHz. Shaded region representing the standard deviation from batch 2.

Table E.2: Full T_1 and T_2 relaxation time dataset for MRI at 300 MHz, from batch 1 and batch 2 with replicates. *E. undae (E), L. mesenteroides* (L), and *P. chlororaphis* (P).

Batch	Replicate	Strain	Day	T1 (ms)	T2 (ms)
1	–	E	0	1018	83.0
1	–	E	1	–	–
1	–	E	3	983	91.0
1	–	E	6	1244	85.5
1	–	E	8	977	91.0
1	–	L	0	1018	83.0
1	–	L	1	–	–
1	–	L	3	1229	86.0
1	–	L	6	1067	91.0
1	–	L	8	1288	89.0
1	–	P	0	1018	83.0
1	–	P	1	–	–
1	–	P	3	1142	86.0
1	–	P	6	1073	89.4
1	–	P	8	1133	87.0
2	R1	E	0	879.6	101.6
2	R1	E	1	1163	84.0
2	R1	E	3	1047	90.0
2	R1	E	6	1088	82.8
2	R1	E	8	1076	89.6
2	R1	L	0	879.6	101.6
2	R1	L	1	1071	85.0
2	R1	L	3	1194	93.4
2	R1	L	6	1251	88.1
2	R1	L	8	1057	95.0
2	R1	P	0	879.6	101.6
2	R1	P	1	1093	84.7
2	R1	P	3	1084	91.8
2	R1	P	6	1187	88.7
2	R1	P	8	1116	89.2
2	R2	E	0	933	98.0
2	R2	E	1	951	91.5
2	R2	E	3	1052	85.4
2	R2	E	6	1013	91.9
2	R2	E	8	1007	91.4
2	R2	L	0	933	98.0
2	R2	L	1	1054	89.0
2	R2	L	3	1106	88.7
2	R2	L	6	1055	94.4
2	R2	L	8	996	97.1
2	R2	P	0	933	98.0
2	R2	P	1	1248	86.9
2	R2	P	3	1051	87.7
2	R2	P	6	1096	93.0
2	R2	P	8	1160	91.4

DEPARTMENT OF, CHEMISTRY AND CHEMICAL ENGINEERING
CHALMERS UNIVERSITY OF TECHNOLOGY
Gothenburg, Sweden
www.chalmers.se

CHALMERS
UNIVERSITY OF TECHNOLOGY